THE MECHANICAL PROPERTIES OF MULTI-YEAR SEA ICE, PHASE I: ICE STRUCTURE ANALYSIS

J.A. Richter-Menge, G.F.N. Cox
and N. Perron

U.S. Army Cold Regions Research
and Engineering Laboratory
72 Lyme Road
Hanover, NH 03755-1290

THE MECHANICAL PROPERTIES OF MULTI-YEAR SEA ICE
PHASE I: ICE STRUCTURE ANALYSIS

by

J.A. Richter-Menge, G.F.N. Cox and N. Perron

U.S. Army Cold Regions Research and Engineering Laboratory
72 Lyme Road
Hanover, New Hampshire 03755-1290

Prepared For

Shell Development Company

And

Minerals Management Service
U.S. Department of the Interior

MECHANICAL PROPERTIES OF MULTI-YEAR SEA ICE

PHASE I: ICE STRUCTURE ANALYSIS

by

J.A. Richter-Menge, G.F.N. Cox and N. Perron

INTRODUCTION

Multi-year pressure ridges present the most significant hazard to arctic offshore structures in exposed areas of the Beaufort and northern Chukchi Seas. It is, therefore, surprising that we know so little about their internal physical characteristics.

When a pressure ridge is first formed it consists of angular, broken blocks of ice. Initially, the blocks are weakly joined together. During the course of the winter, the ridge begins to consolidate. In the summer, both the top and bottom of the ridge undergo ablation and become rounded in appearance. Meltwater permeates the ridge, flowing into void spaces. If the ridge survives the summer melt and is present the following winter it is called a multi-year ridge. At this point the ridge is massive, with few or no voids, and has a characteristically low salinity. On the surface of the ridge, individual blocks of ice are no longer discernible. Instead, the ridge is rounded and hummocky. A split multi-year ridge will reveal that the internal structure of the ridge still maintains its blocky nature. This history of formation can result in large variations of the ice type and crystal orientation in ice samples taken from a multi-year ridge.

A joint government-industry study was initiated to systematically examine the structure and mechanical properties of ice samples taken from multi-year pressure ridges. The first phase of the program included field sampling in the southern Beaufort Sea. Ten different pressure ridges were sampled and we obtained a continuous, vertical multi-year ridge core specifically for detailed structural analysis. A total of 220 uniaxial constant-strain-rate compression tests were performed on the vertically cored ice samples from the ten ridges. All of these test samples were loaded in the vertical direction. The results from these tests indicated that there were large variations in the peak compressive stress for a given test condition. In order to obtain more confidence in the tests results, it was necessary to explain this variance. Preliminary work, described in the Phase I final report (Cox et al., 1984), indicated that the main factor contributing to variations in the strength from test to test was associated with the extreme local variability of ice structure within a ridge. This large variation in ice structure was also observed in the continuous ridge core. It became apparent that a complete and useful analysis of our data, which included an explanation of the strength variations, would require careful structural interpretation of each test sample. It is the results of this structural examination that are presented in this report. Note that the results of this study on multi-year ridge ice samples also provide information on the compressive strength of individual ice types including columnar and granular.

While the mechanical testing of individual multi-year ridge samples provides important strength parameters, we must also understand how to apply the results on a larger scale. This requires information on the internal composition of multi-year ridges. We should pay particularly close attention to the amount of columnar ice in the ridges studied and the orientation of the crystals in this columnar ice. Studies on first year sea ice by Peyton (1966), Wang (1979) and Richter-Menge et al. (in prep.) have already established the fact that columnar sea ice behaves anisotropically under a variety of loading conditions. The influence of this anisotropy on the large-scale loading behavior of a multi-year ridge may vary depending on the number and arrangement of columnar ice blocks within the ridge. This information is important for the development of constitutive models to predict ridge ice loads on offshore structures and vessels.

Ice samples and a continuous vertical core were also collected from a presumably undeformed multi-year floe during the first phase of this program. The multi-year floe ice samples were used to develop the tension, constant load and triaxial testing techniques used extensively in the second phase of the program. The continuous core was obtained for detailed structural analysis.

This report presents the structural analysis of the Phase I multi-year pressure ridge and multi-year floe test samples and the continuous ridge core. Interpretation of the test results with respect to ice structure is also developed in this report. A discussion of the field sampling program the tests results and analyses, and the structural analysis of the continuous multi-year floe core are presented in a companion report, "Mechanical Properties of Multi-Year Sea Ice, Phase I: Test Results" (Cox et al., 1984). The development of suitable sample preparation and testing techniques is described in a second report, "Mechanical Properties of Multi-Year Sea Ice: Test Techniques" (Mellor et al., 1984).

SAMPLE ANALYSIS

The structural characteristics of the continuous multi-year ridge core and the Phase I ridge and floe test samples were evaluated by preparing ice thin sections according to the techniques described in Weeks and Gow (1978). The test samples were sectioned after testing. Horizontal thin sections were prepared from the top, middle and bottom of the tested samples as shown in Figure 1. The remainder of the sample was sectioned vertically in two cuts, one perpendicular to the other. If a sample was destroyed during the test, end pieces taken immediately adjacent to the sample were used to interpret the structural composition of the sample. The ice type was determined by studying the photographs of the horizontal and vertical thin sections taken between crossed polaroids.

The ice type in each sample was then described according to the multi-year pressure ridge ice structural classification scheme summarized in Table 1. Figure 2 shows a series of thin sections, photographed between crossed polaroids, that illustrates the principal structural characteristics of each ice type. This structural classification scheme is descriptive in nature and divides the ice samples into three major ice texture categories; granular, columnar, or a mixture of columnar and granular ice. It is inappropriate to use a genetically based classification method such as those proposed by Michel (1978) and Cherepanov (1974) for the multi-year ridge samples because these systems do not consider deformed ice types. Both of the classification methods mentioned require some knowledge of the

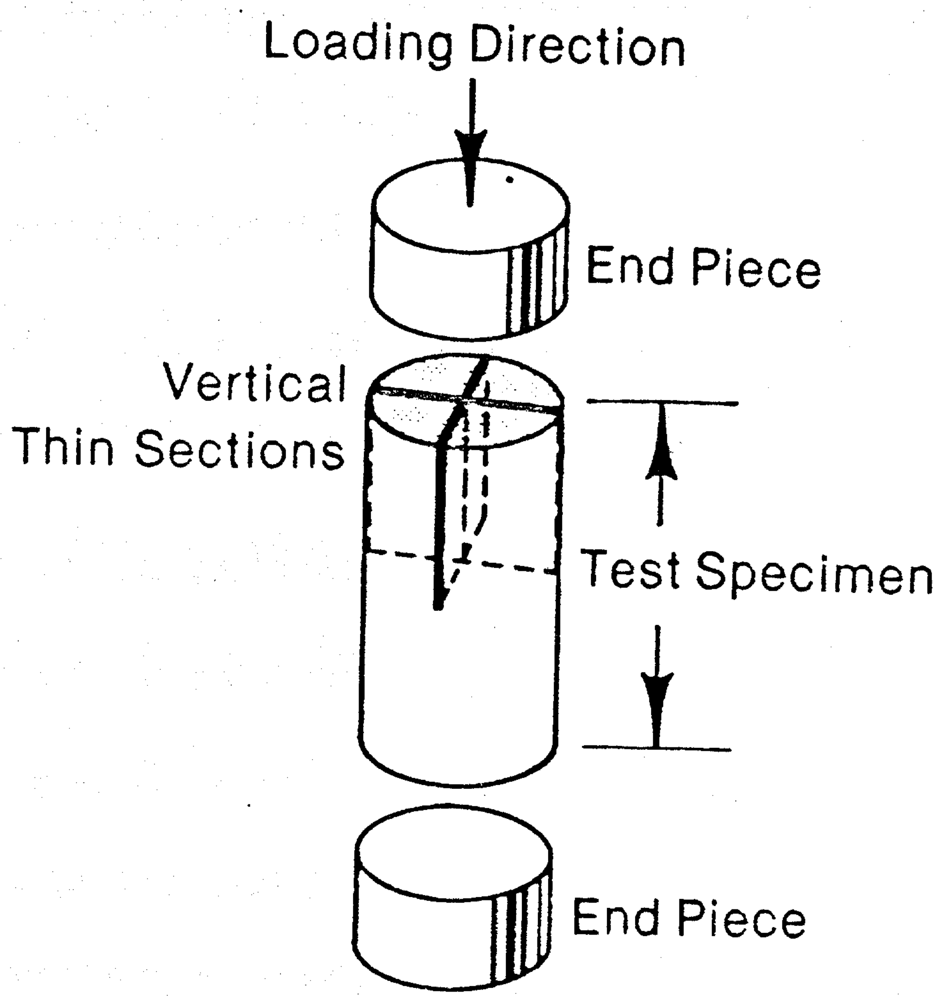

Figure 1. Sections used in the analysis of the structural characteristics of the tested ice samples.

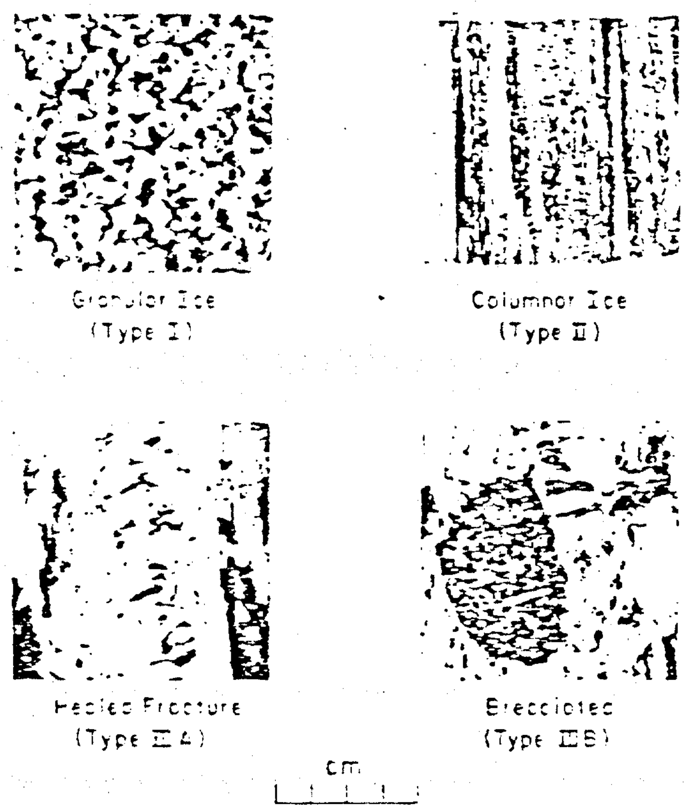

Figure 2. Structural characteristics of multi-year ice types.

ice origin; because the ridge ice is deformed, the origin of ice type in a ridge ice sample is difficult to establish.

We can postulate however, the possible modes of origin of each ice texture type. Granular ice may be derived from snow or slush ice, from frazil, from the granulation of the sheet ice during the ridge building process, or from freezing in the void spaces in the ridge during consolidation. Columnar sea ice is probably largely derived from the parent ice sheet incorporated into the ridge during its formation. It may also form at the bottom of the ridge by congelation growth. Meltwater ponds formed and refrozen on the parent ice sheet before deformation took place are the most likely source of the columnar freshwater ice (Type IIC) observed in

Table 1. Structural classification scheme for multi-year pressure ridge ice samples.

Ice Type	Code	Structural Characteristics
Granular	I	Isotropic, equiaxed crystals
Columnar	II	Elongated, columnar grains
	IIA	Columnar sea ice with c-axes normal to growth direction; axes may or may not be aligned
	IIC	Columnar freshwater ice
Mixed	III	Combination of Types I and III
	IIIA	Largely Type II with granular veins
	IIIB	Largely Type I with inclusions of Type I or II ice (brecciated ice)

the ridge ice samples. The mixed ice is the result of the ridge building and consolidation process. Type IIIA ice includes healed fractures and

Type IIIB ice is the cataclastic end product of ice blocks being ground together during the ridge building process. These same ice types have also been observed in multi-year floes, sampled in the Fram Strait region of the Greenland Sea (Tucker et al., 1985). The Fram Strait is the major outflow region for first- and multi-year ice formed in the Arctic Basin.

If a sample was classified as columnar, or contained large fragments of columnar ice, the ice thin sections were analyzed on the Rigsby Universal Stage (Langway, 1958). These measurements provided us with information on the mean angle between the crystallographic c-axes and the load direction (σ:c) and the degree of alignment of the c-axes (° spread). We also used the thin section analysis to determine the angle between the columns or direction of elongation of the crystals and the vertical (σ:z). In an undeformed sheet of first-year sea ice the crystals are elongated vertically (σ:z = 0°), parallel to the growth direction of the sheet. The c-axes of these crystals are usually located in the horizontal plane of the ice sheet, normal to the elongation direction of the crystals. By observing the orientation of the crystallographic c-axes and the direction of elongation of the crystals in the ridge ice samples, we can determine the arrangement of some of the columnar fragment of first-year sea ice that have been incorporated into a ridge. The photographed thin sections of each sample helped to confirm these measurements. Note that thin sections taken perpendicular to the load, which was applied along the vertical axis of the sample, were used for these crystallographic measurements to avoid misinterpretation as a result of apparent dip and plunge. Also, a number of samples could not be crystallographically analyzed since their thin

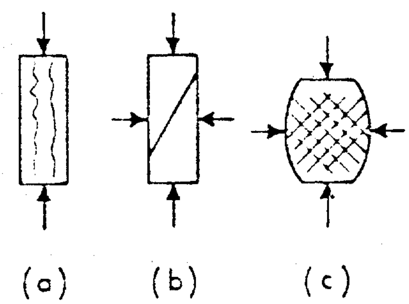

Figure 3. Typical compressive failure modes; (a) longitudinal splitting, (b) shear fracture, and (c) multiple shear fractures.

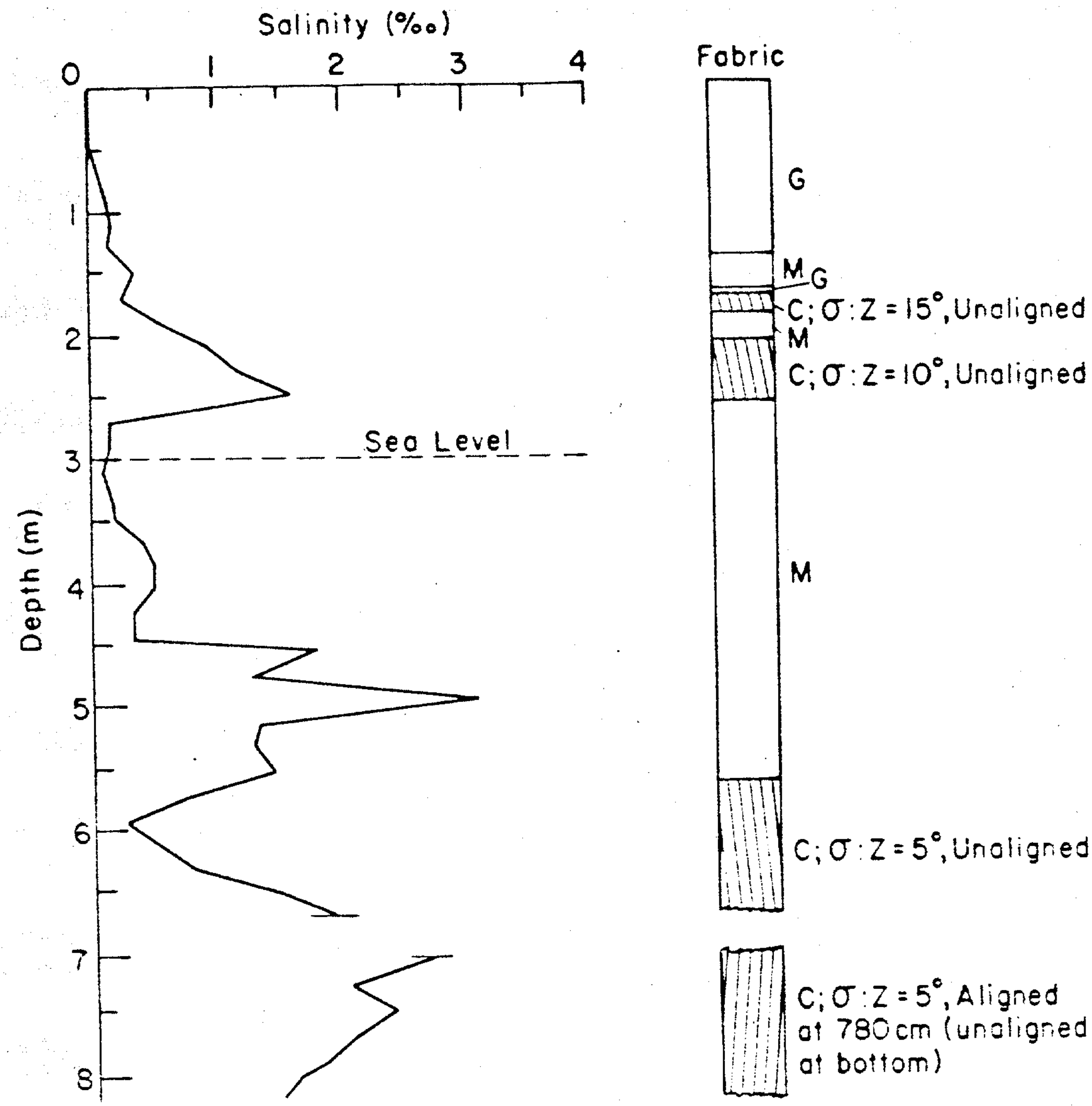

Figure 4. Salinity and schematic structural profile for the Phase I continuous multi-year pressure ridge core. G = granular ice, C = columnar ice, M = mixed granular and columnar ice.

temperature. In Phase I of the mechanical properties of multi-year sea ice program the tests were conducted at two temperatures (-5 and -20°C) and two strain rates (10^{-3} and 10^{-5} s^{-1}). In Table 2, we have summarized the number of samples classified according to the three main ice texture categories at each test condition. The percentage of a given ice type (granular, columnar or mixed) is consistent from one test condition to another. The most commonly found ice type by far is the mixed columar and granular ice, indicating that the ridge building process is extremely dynamic.

Table 2. Summary of the number of columnar, granular and mixed ice samples at each Phase I test condition.

	-5°C		-20°C		
	10^{-3} s^{-1}	10^{-5}	10^{-3}	10^{-5}	Total
Granular	5	7	1	1	14 (6%)
Columnar	17	14	8	8	47 (21%)
Mixed	47	51	31	32	161 (73%)
Total	69	72	40	41	222

In Table 3, the number of columnar samples tested in each of the 10 sampled ridges is given. We have included as columnar samples those samples classified as columnar and those classified as mixed which are made up of greater than or equal to 80 percent columnar ice. As we will discuss later, these mixed ice samples behave similarily to the columnar ice samples. In the last column of Table 3, we have also listed the number of columnar samples that were crystallographically measured on the Rigsby Universal Stage to determine σ:c and σ:z. We were unable to define these parameters for all columnar samples due to the excessive damage experience by a number of thin sections during storage.

Table 3. Columnar ice samples tested in Phase I. These samples include both columnar and mixed samples with greater than or equal to 80% columnar ice.

Ridge no.	Total number of samples tested	Total number of columnar samples	% columnar samples	Number of columnar samples oriented
1	23	13	57	12
2	24	4	17	4
3	22	3	14	1
4	22	6	27	6
5	22	5	23	3
6	12	0	0	0
7	23	6	26	4
8	24	15	63	13
9	24	1	4	0
10	24	8	33	7
	220	61	28	50

As we would expect, the amount of columnar ice varies from ridge to ridge. This variation is due to the differences in the mode of formation of the ridges. As described in Kovacs and Mellor (1974), a first-year ridge formed by compression contains large, unconsolidated blocks of columnar sheet ice. The ice in a ridge formed by shearing, on the other hand, is highly fragmented and very compact. So we would expect to see a higher percentage of columnar ice samples in a multi-year pressure ridge initially formed by compression than in one formed in shear. Many of the ridges do contain a significant amount of anisotropic columnar ice. In a total of 220 tested samples 61, or 28%, of the samples were made up of greater than or equal to 80% columnar ice.

A frequency histogram of the number of columnar samples in a given σ:z orientation is presented in Figure 5. The large number of low σ:z angle measurements in Figure 5 indicates that in a majority of these

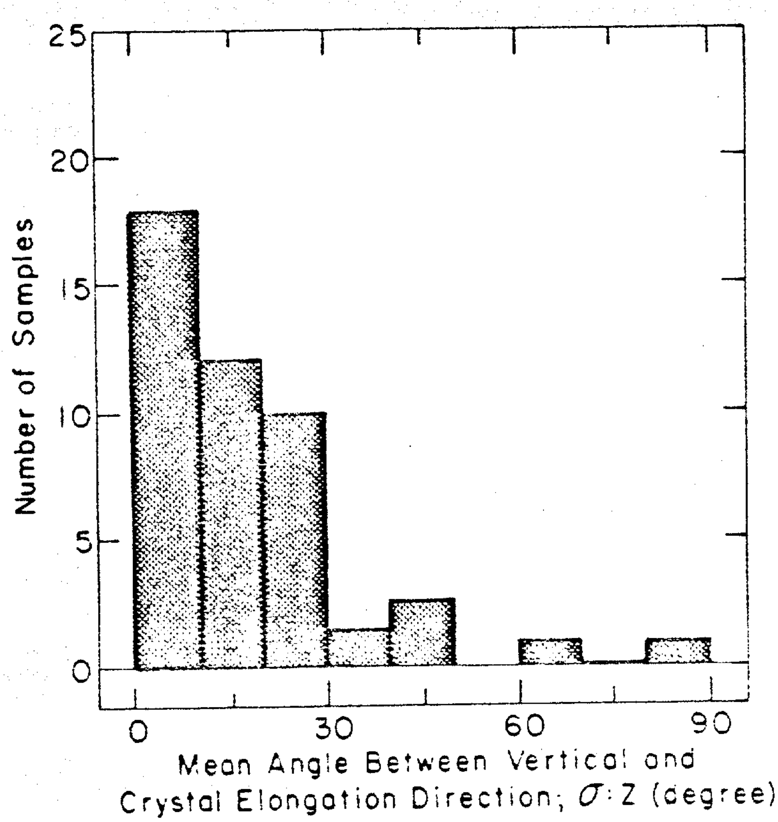

Figure 5. Frequently histogram of the number of Phase I columnar ridge ice samples in a given orientation.

columnar samples the direction of elongation of the crystals was near vertical (σ:z ≈ 0°).

These observations along with the measurements made on the continuous core indicate that many multi-year pressure ridges contain a significant amount of columnar ice and that in much of this columnar ice the direction of elongation of the crystals may be close to vertical. That is, blocks of first-year sea ice, incorporated into the ridge during its formation, lie in a near-horizontal position. In this position the large columnar blocks are most stable. As a result of this apparent preferential block orientation, the majority of vertically cored columnar ridge samples are loaded nearly parallel to the direction of crystal elongation (σ:z=0°). This is the hard fail direction for columnar ice. Horizontal columnar samples would tend to have an angle of 90° between the applied compressive load and the direction of crystal elongation, giving a lower strength. Work by Peyton (1966) has shown that the compressive strength can differ between the vertical and horizontal loading conditions by as much as a factor of three, depending on the σ:c angle.

Accordingly, care must be taken when applying mechanical property test data from multi-year pressure ridges to the design of arctic offshore structures and vessels. The mean compressive strength obtained from a series of tests on vertical ridge samples is likely to be higher than the mean value obtained from horizontal samples (Cox et al., in press; Richter-Menge and Cox, 1985). Using the ice strength data from vertical ridge samples may be conservative in horizontal ridge loading problems. Note that the degree of variation between the mean strength obtained from vertical and horizontal ridge samples is strongly dependent on the amount of columnar ice in the test series and the orientation of the columnar crystals.

In Figures 6a through d, the compressive strength of the multi-year ridge samples is plotted against sample porosity and the structural classification is indicated for each test specimen. Ice porosities were calculated from the salinity, density and temperature of each sample using equations developed by Cox and Weeks (1983). Upon initial inspection of Figure 6, the results seem to vary depending on the given test condition. For instance, at a strain rate of 10^{-3} s^{-1} and temperature of -5°C (Fig. 6a) there is a group of high strength columnar samples. The granular samples tested at this condition are lower in strength than the mixed samples. Samples tested at the same temperature but at a slower strain rate of 10^{-5} s^{-1} (Fig. 6b) also include a group of high strength columnar samples. The granular samples at this test condition however, have a higher compressive strength than the mixed samples. Finally, the samples tested at a temperature of -20°C indicate that none of the columnar samples have strengths significantly higher than the mixed ice samples. In fact, at a strain rate of 10^{-5} s^{-1} (Fig. 6d) there is a group of low strength columnar samples.

Much of this apparent variation of the results between test conditions can be explained in general terms using Figures 7 and 8. In these figures we have made separate plots of the strength and porosity of the columnar and mixed samples, respectively. On both plots we have also included all of the crystallographic data on the measured angle between the vertical and direction of elongation of the crystals (σ:z), the angle between the load and the crystallographic c-axes (σ:c), and the spread or degree of

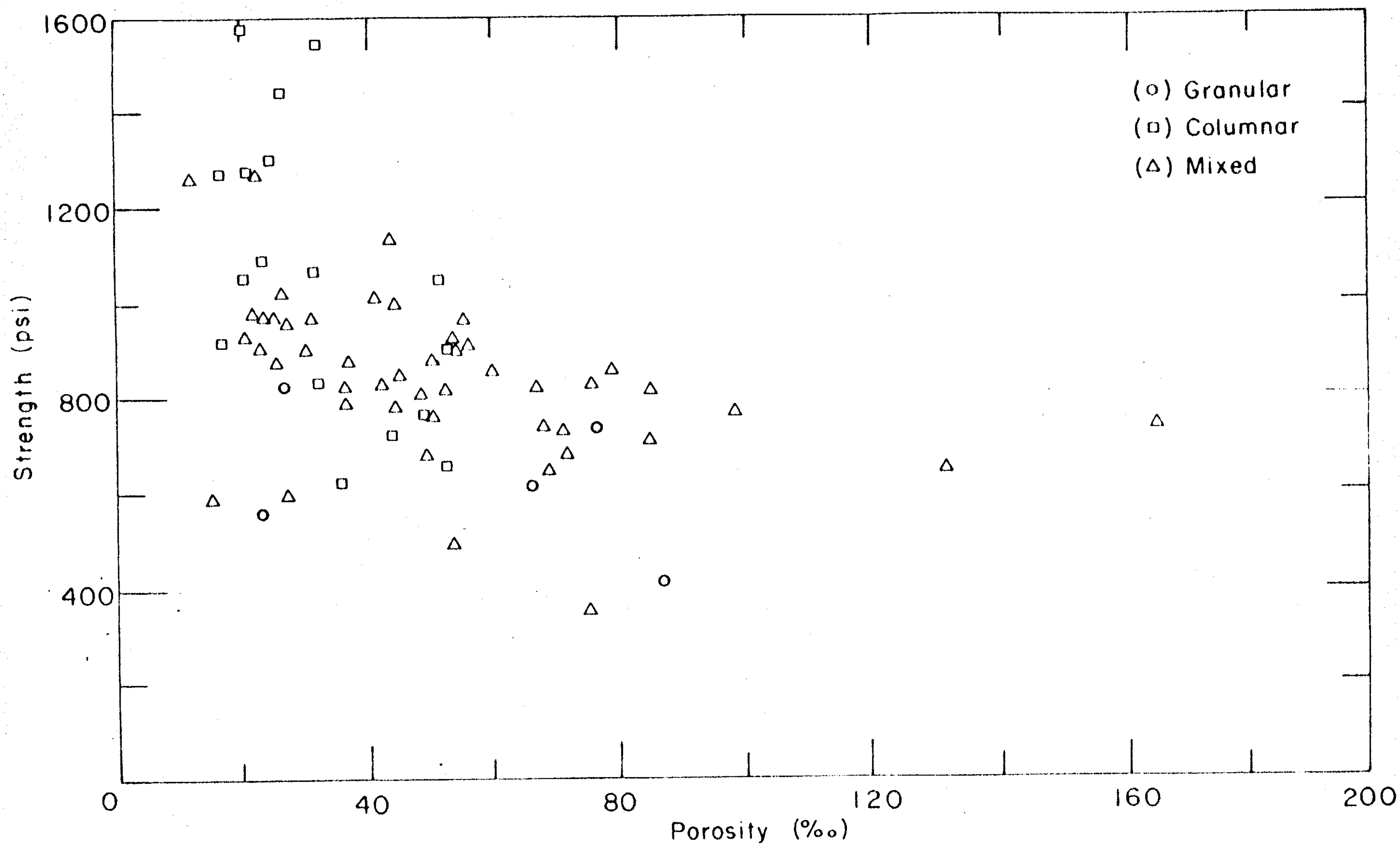

a. Tests conducted at 10^{-3} s^{-1} and -5°C.

Figure 6. Uniaxial compressive strength versus pososity for all Phase I, ridge ice samples with the structural classification indicated for each sample.

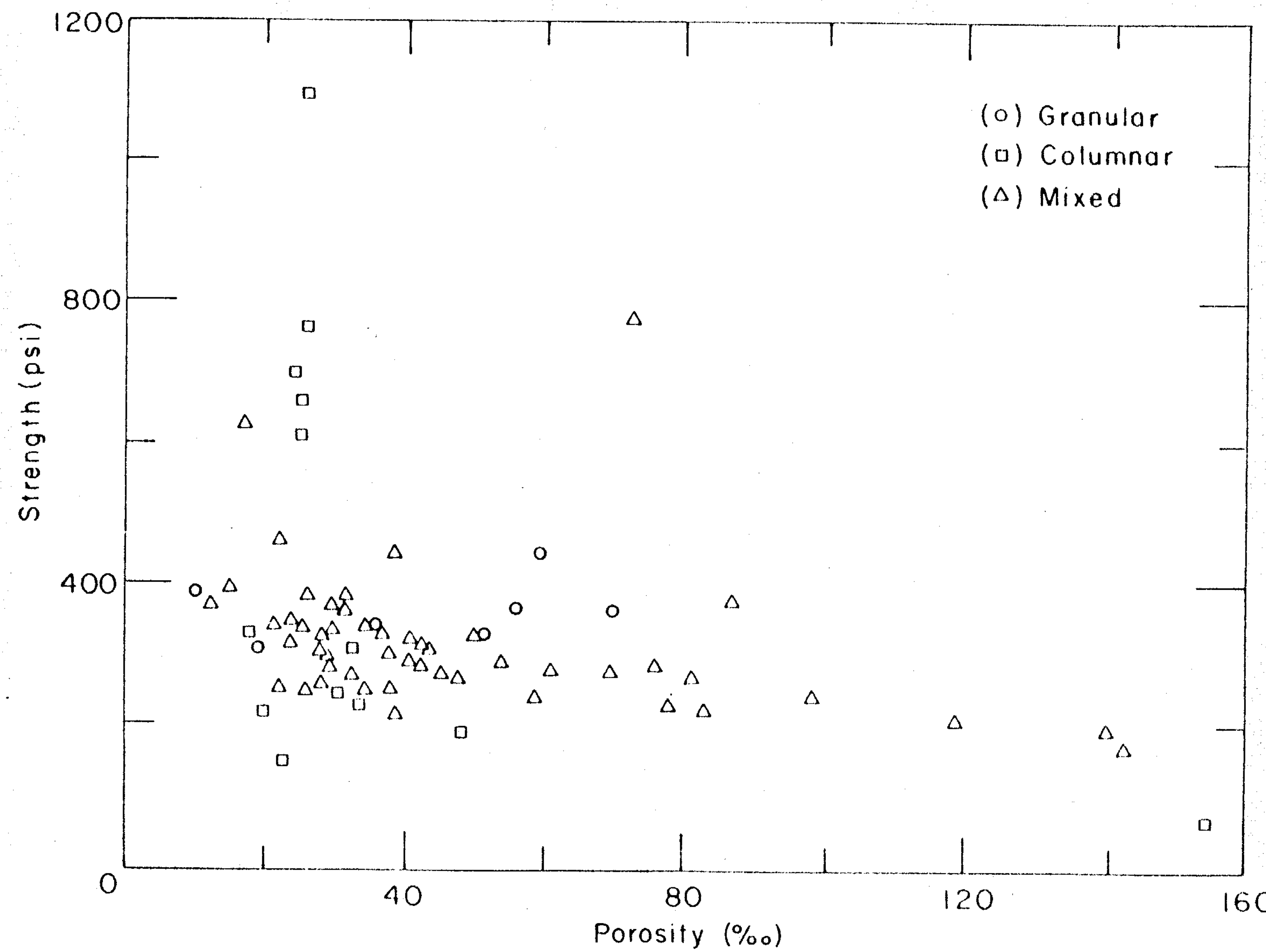

b. Tests conducted at 10^{-5} s^{-1} and -5°C.

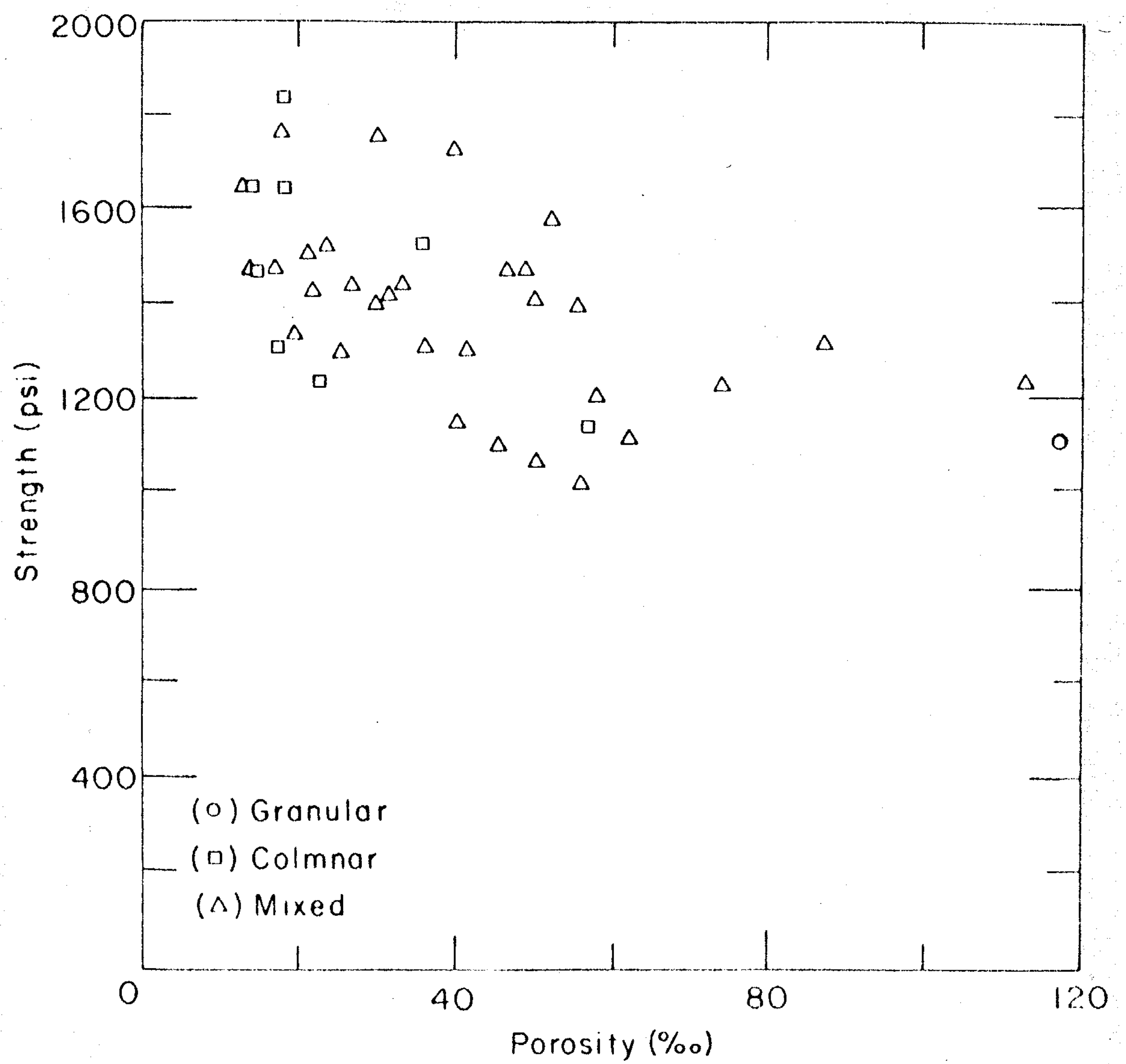

c. Tests conducted at 10^{-3} s^{-1} and $-20°C$.

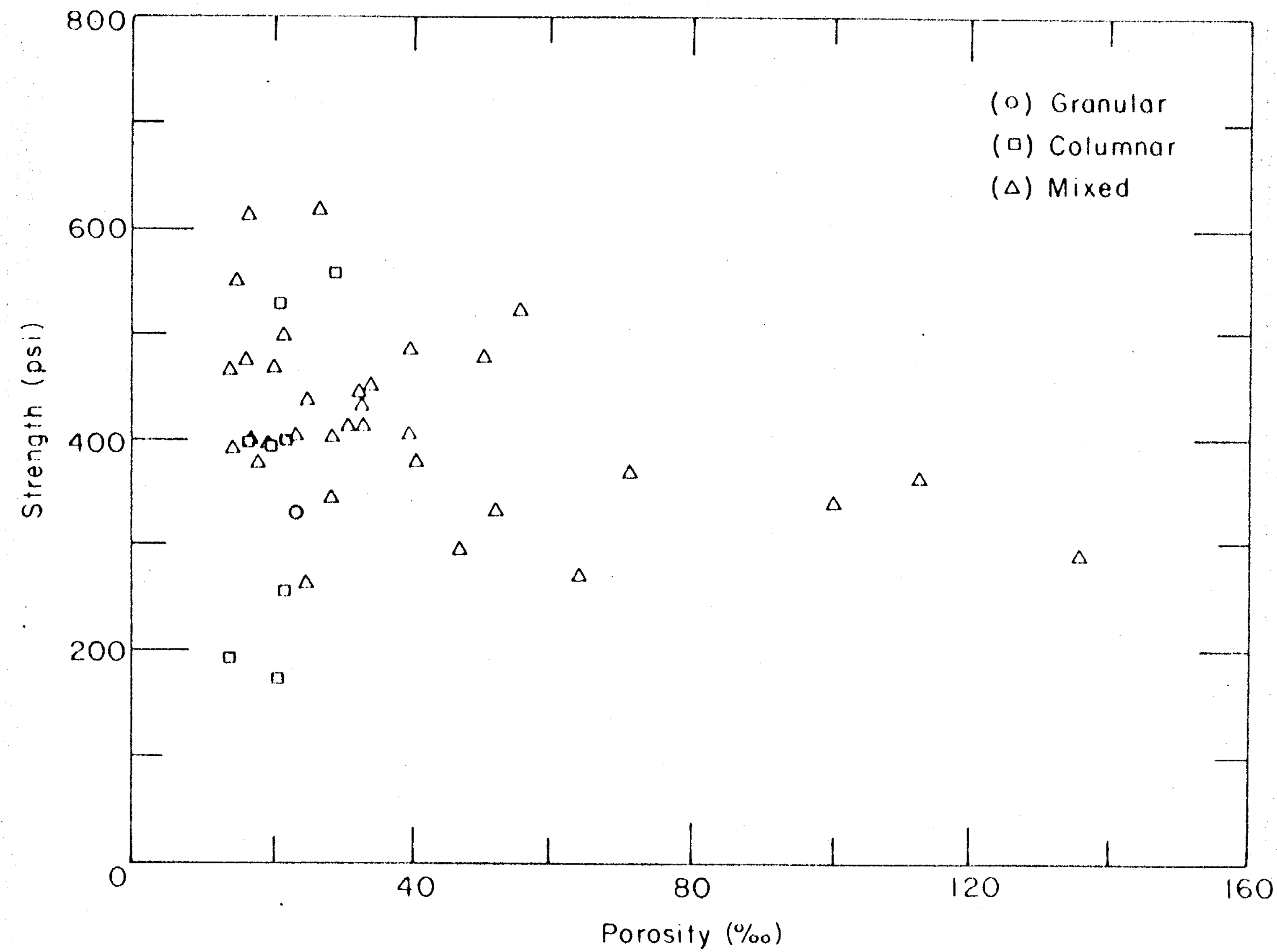

d. Tests conducted at 10^{-5} s^{-1} and -20°C.

alignment of the c-axes in the plane perpendicular to the elongation direction. Note that in Phase I the compressive load was in the vertical direction parallel to the cylindrical axis of the vertically cored sample. For the mixed ice samples (Fig. 8) we have also included the percentage of columnar ice in the sample.

At strain rates of 10^{-3} and 10^{-5} s^{-1} and a temperature of -5°C (Fig. 7a and b), the high strength columnar samples are oriented with the direction of crystal elongation near vertical or parallel to the load (σ:z$\leq$10°) and that the degree of c-axes alignment is relatively small ($\leq$ 50°). This is the hard fail direction in ice (Peyton, 1966). These columnar samples also have a low porosity. In Figure 7c and d on the other hand, there are few columnar samples with these high strength characteristics. Correspondingly, we do not have an isolated group of higher strength columnar samples at these test conditions. In general, the strength of the vertically loaded columnar samples drops off rapidly as σ:z increases. As we approach a σ:z angle of 45° the compressive strength becomes extremely low. At σ:z = 45°, the basal planes of the ice crystals (plane of weakest shear strength) coincide with the plane of maximum shear (45° from loading direction) and the sample shows a lower resistance to failure. This results in a relatively low compressive strength. The reduction in strength is more dramatic for those samples with a small spread in the c-axes alignment. Figure 7d illustrates the low strength of columnar samples at this orientation. At this test condition there are a group of three columnar samples with strengths lower than the mixed samples.

Ideally, we would like to use both the σ:z and σ:c angle to determine the exact location of the basal plane with respect to the failure plane in

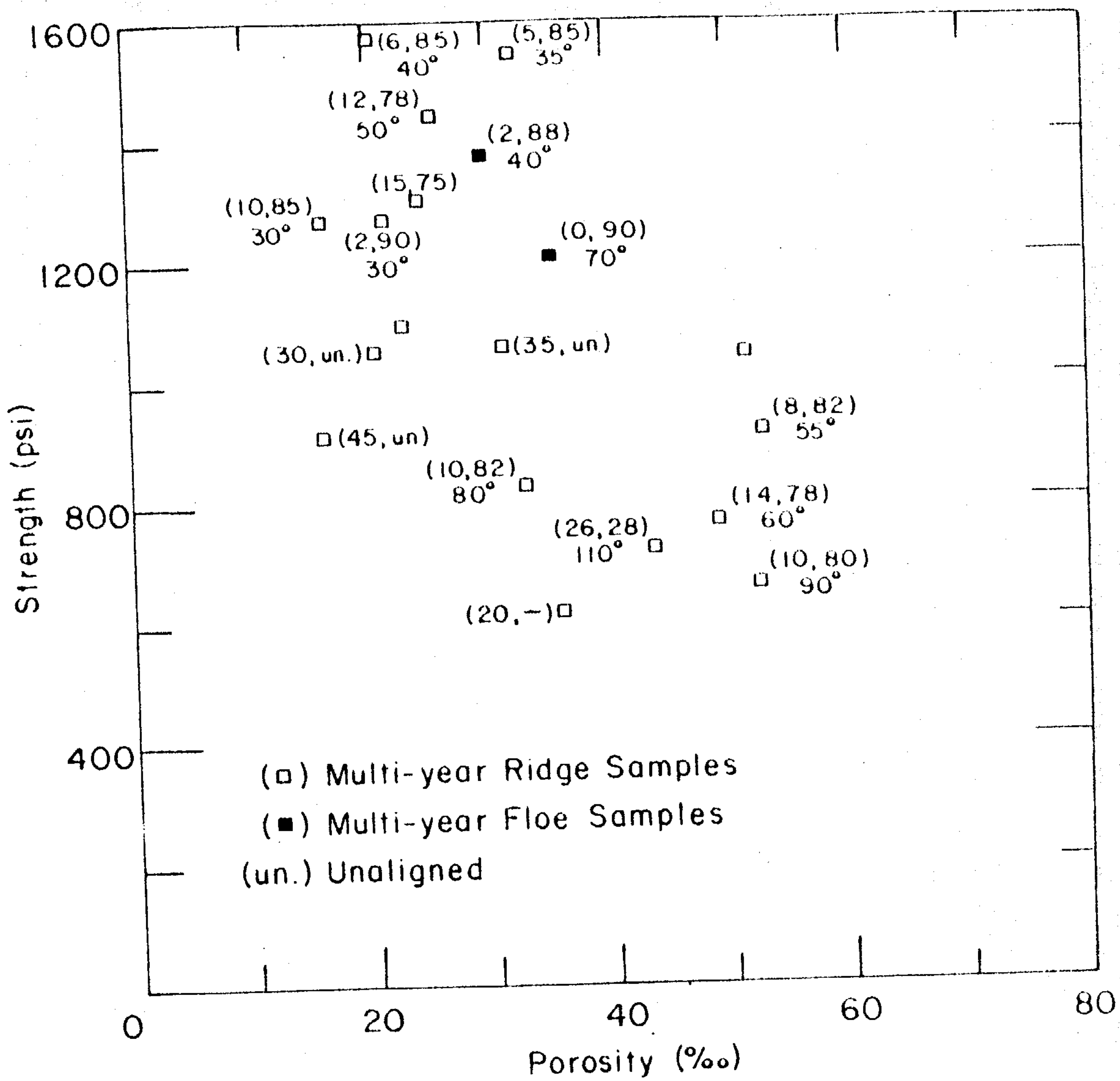

a. Tests conducted at 10^{-3} s^{-1} and $-5°C$.

Figure 7. Uniaxial compressive strength versus porosity for Phase I columnar ridge and floe ice samples. Crystallographic measurements indicated next to each sample: (σ:z, σ:c), °spread.

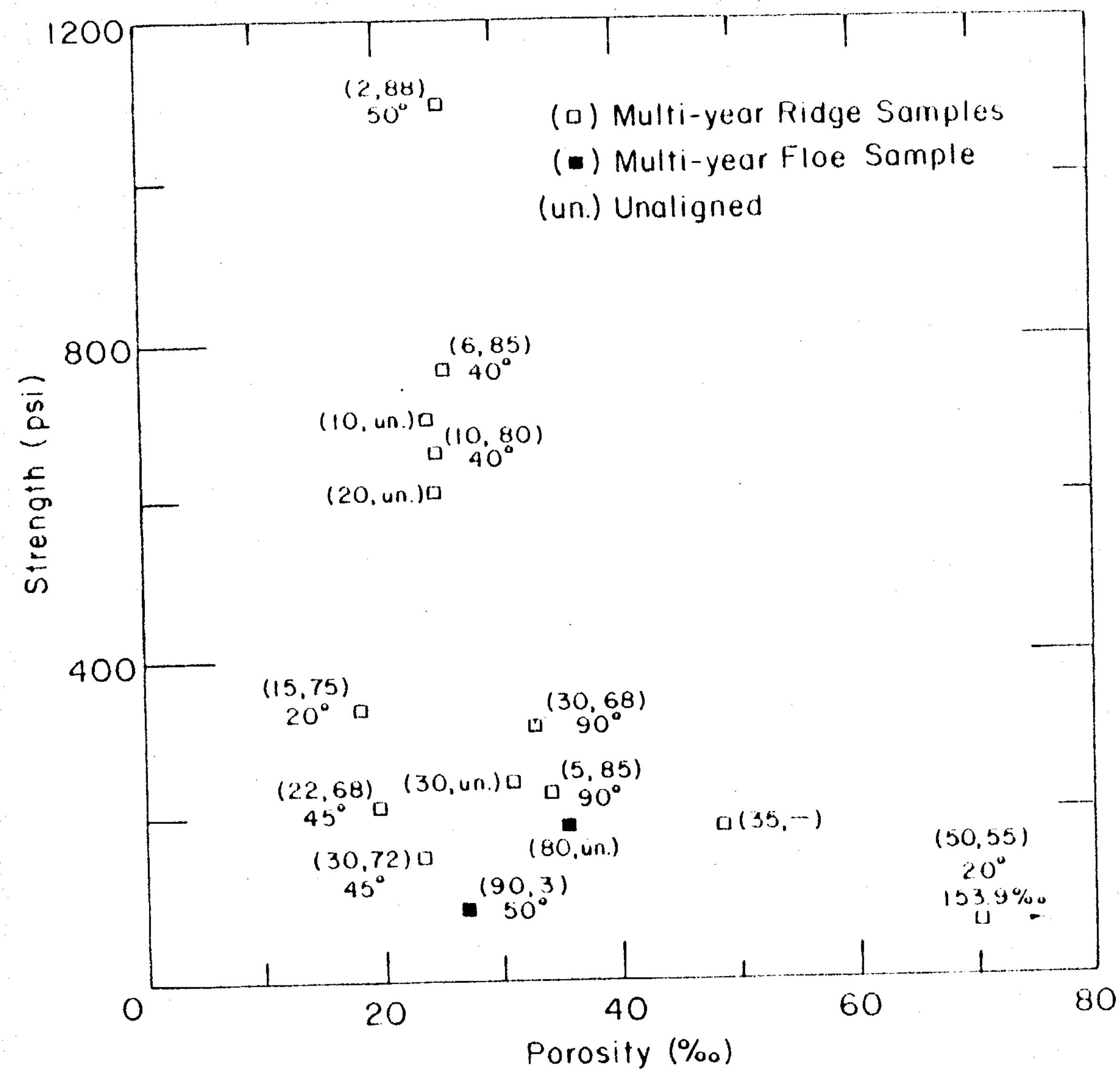

b. Tests conducted at 10^{-5} s^{-1} and $-5°C$.

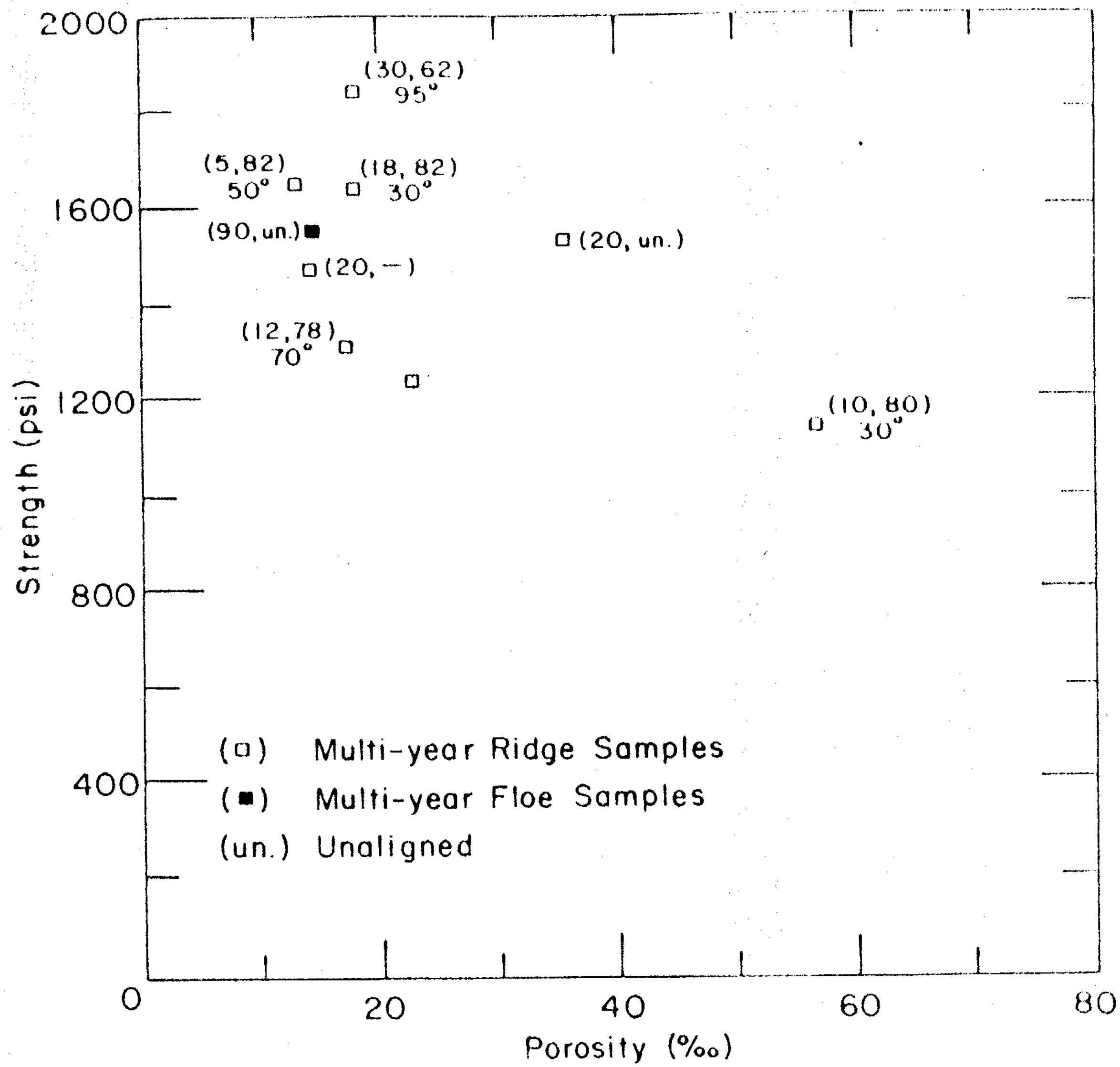

c. Tests conducted at 10^{-3} s^{-1} and $-20°C$.

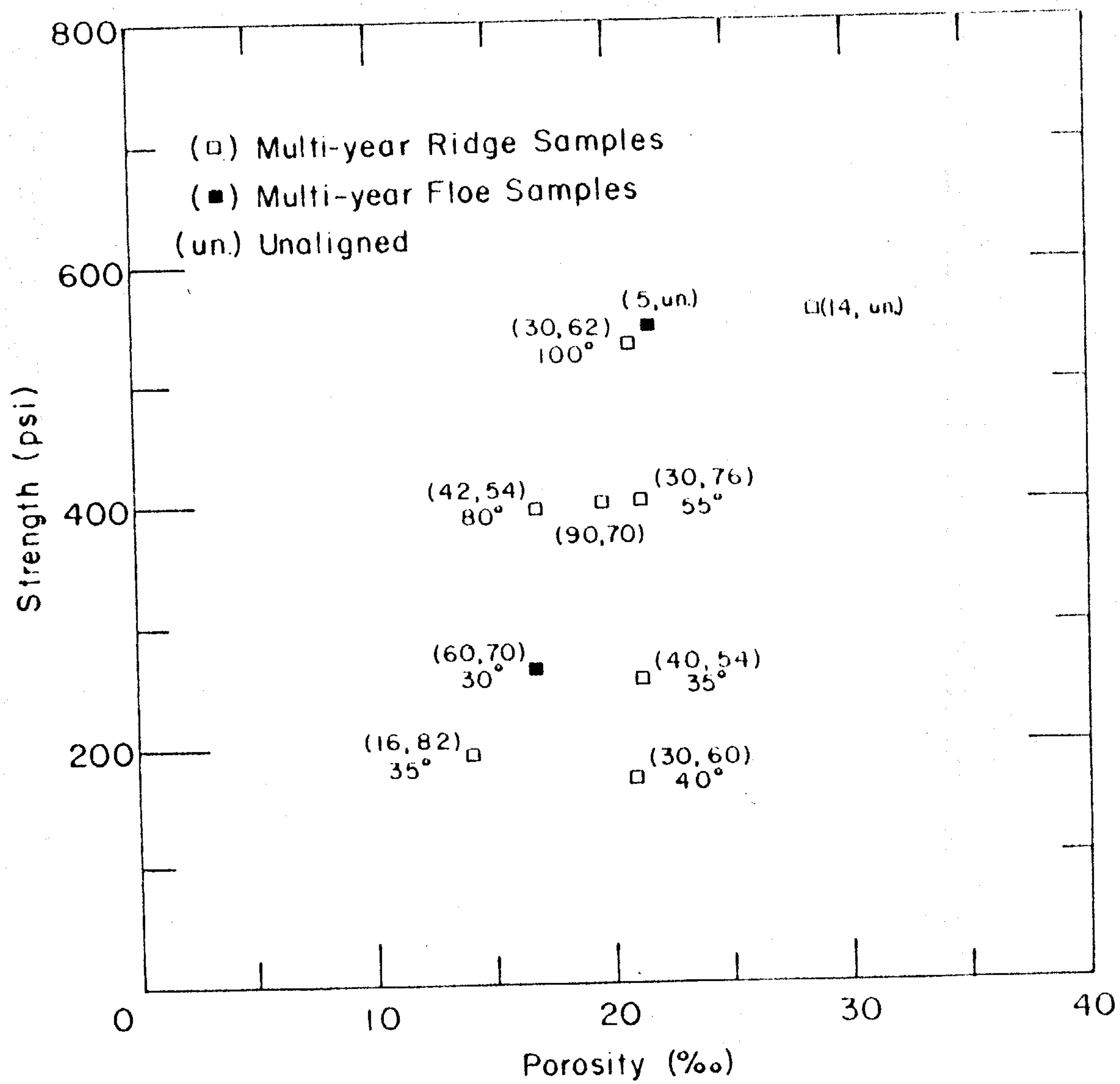

d. Tests conducted at 10^{-5} s^{-1} and $-20°C$.

all of our columnar samples. This would allow us to more completely understand the influence of ice crystal orientation on the compressive strength. This determination would require knowledge of the location of the thin section, used in the angle measurement, relative to the failure plane. In Phase I, this information was not documented.

The compressive strength versus porosity plots for the mixed ice samples (Figs. 8a-d) indicate that as a result of the influence of the columnar fragments in the mixed samples, those samples with a high percentage of columnar ice lie on the perimeter of the strength versus porosity band. In fact, the mixed samples with a high percentage of columnar ice ($\geq$ 80%) behave like the columnar ice samples such that samples with a σ:z angle near zero and high degree of c-axes alignment have a high compressive strength (Fig. 8d). Those with a σ:z angle of 45° have a low strength. Mixed ice samples with a low percentage of columnar ice have strengths close to the mean strength at a given test condition. The orientation of the columnar fragments also affects the deformational characteristics of the mixed ice samples. If the columnar ice fragments are oriented with the crystal elongation parallel to the load (σ:z=0°) the sample deforms via the granular material surrounding the columnar fragments. As the angle between the direction of crystal elongation and the load approaches 45°, the majority of the sample deformation takes place in the columnar fragments. Recall, that at an angle of 45° the basal planes of the columnar ice crystals are in a favorable orientation for failure since they coincide with the plane of maximum sheer.

The influence of columnar fragment orientation on both the strength and deformation characteristics of the mixed ice samples is particularly

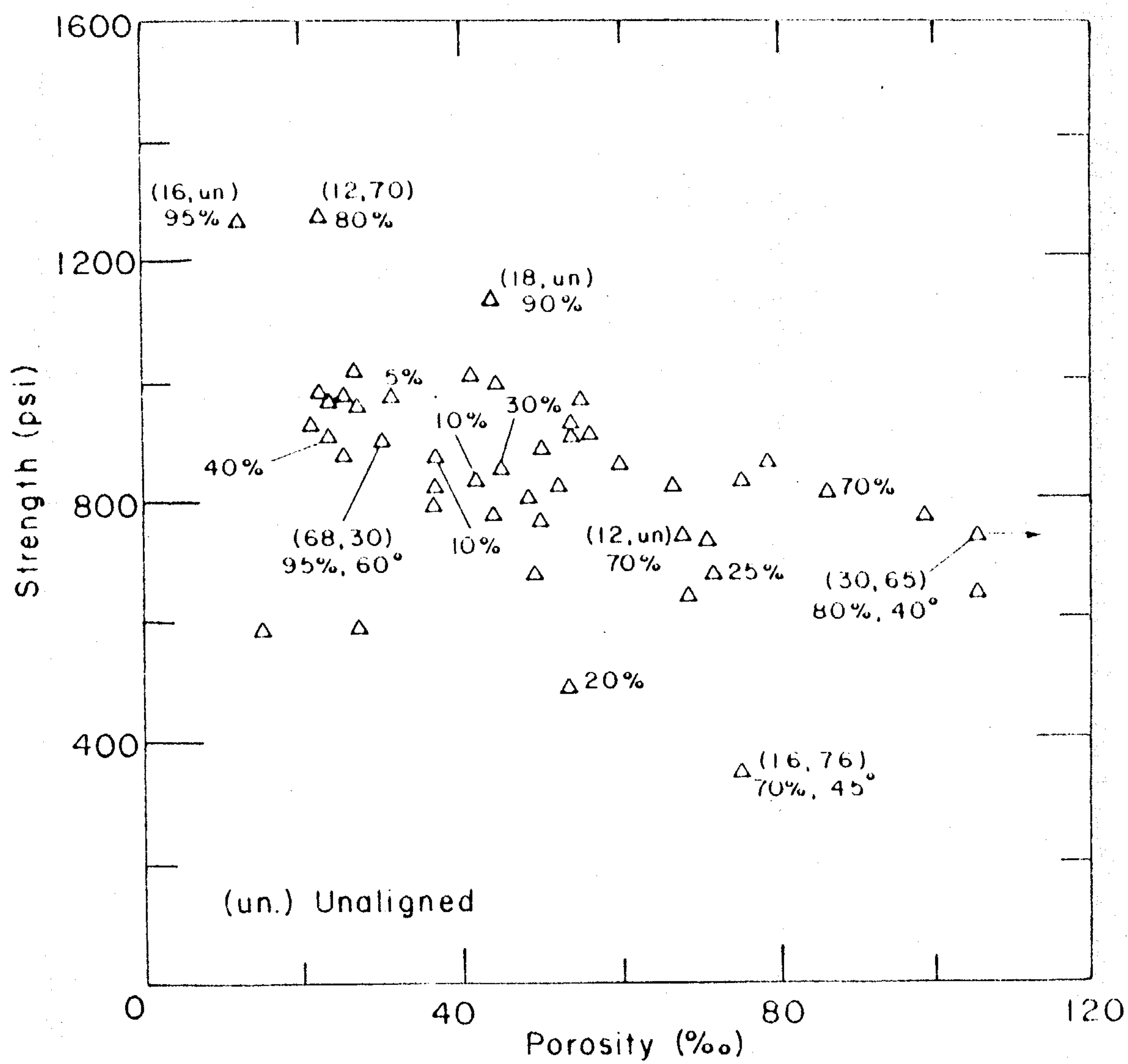

a. Tests conducted at 10^{-3} s^{-1} and -5°C.

Figure 8. Uniaxial compressive strength versus porosity for Phase I mixed ridge ice samples. Crystallographic measurements indicated [illegible]

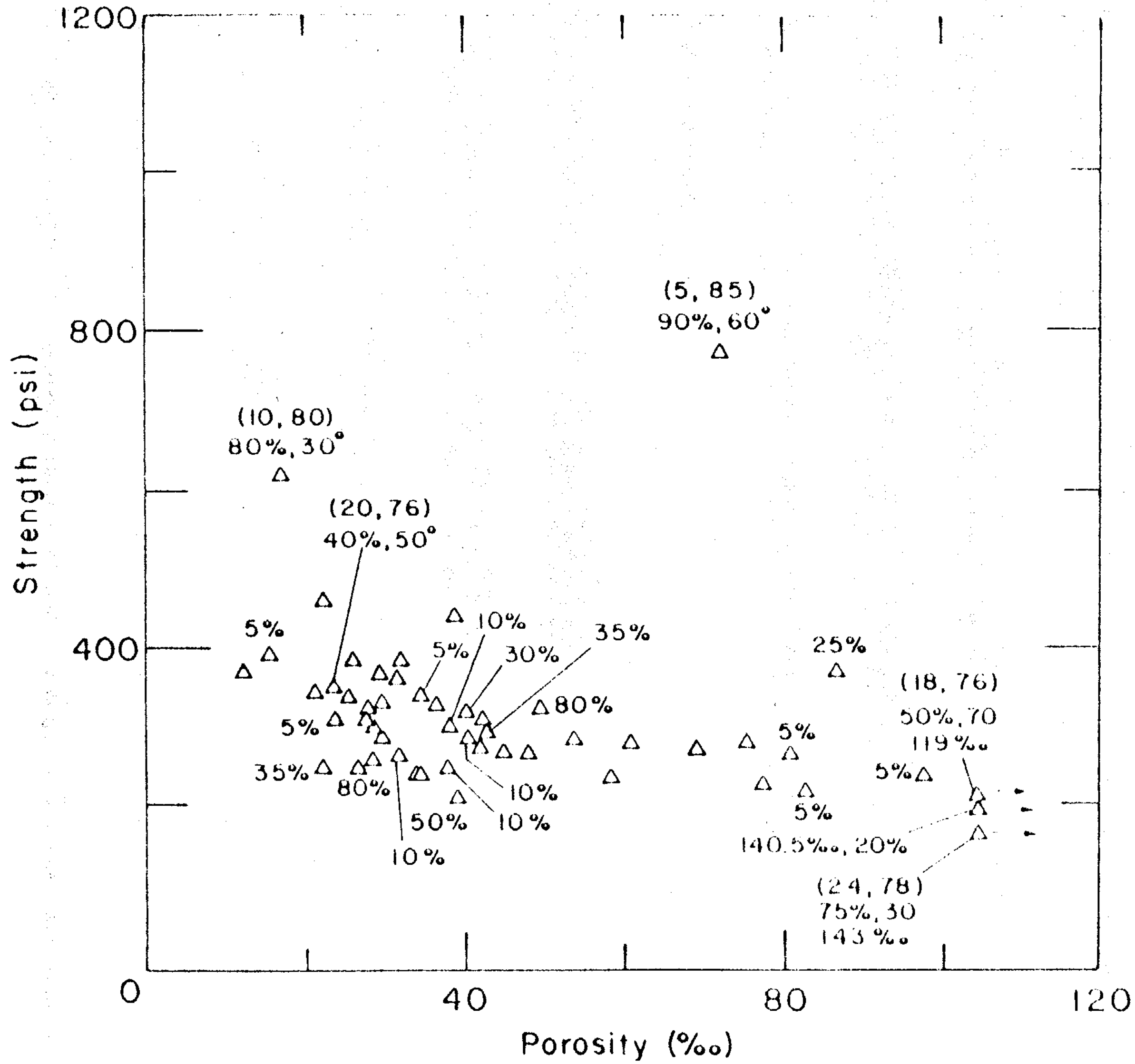

b. Tests conducted at 10^{-5} s^{-1} and $-5°C$.

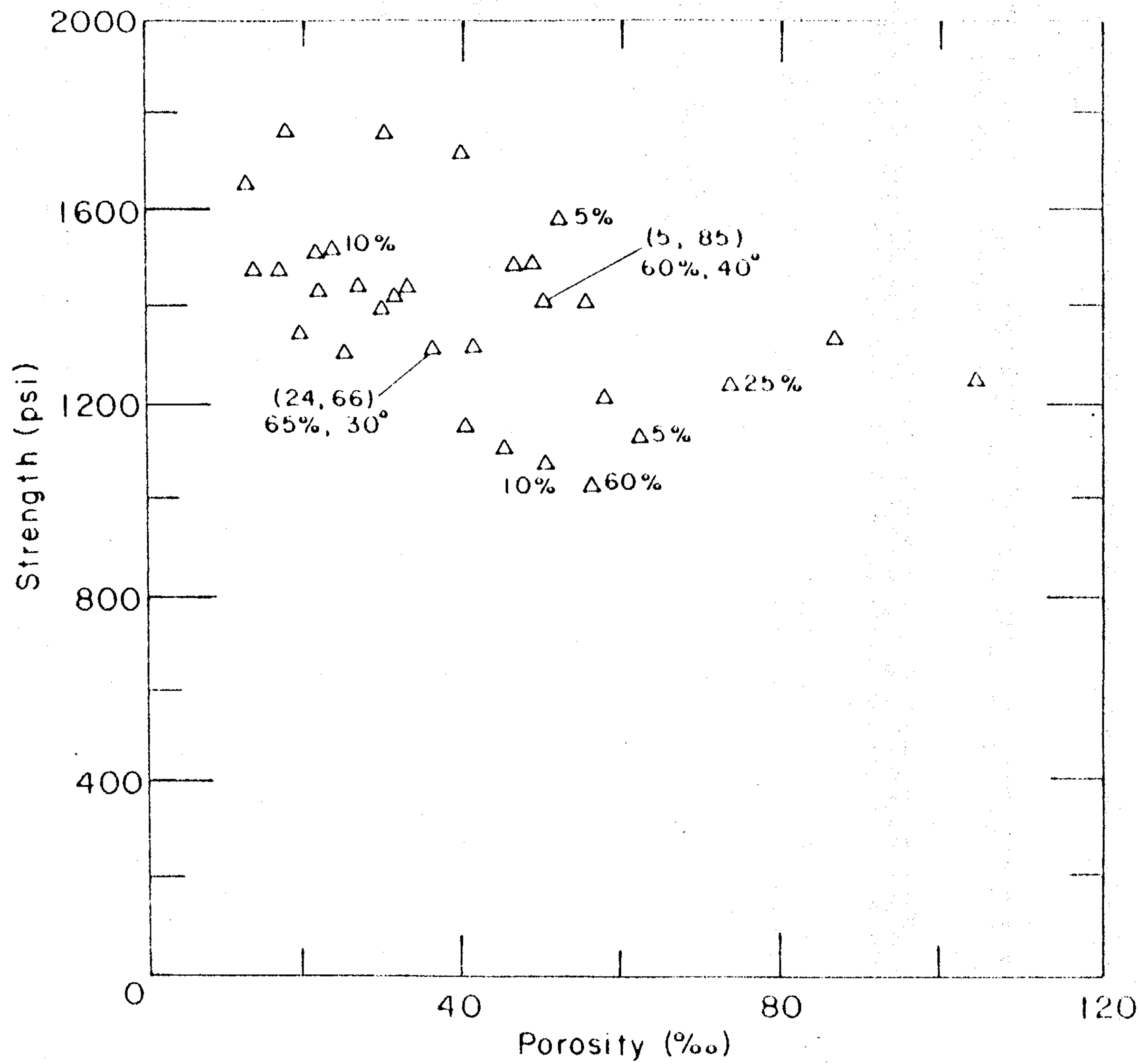

c. Tests conducted at 10^{-3} s^{-1} and −20°C.

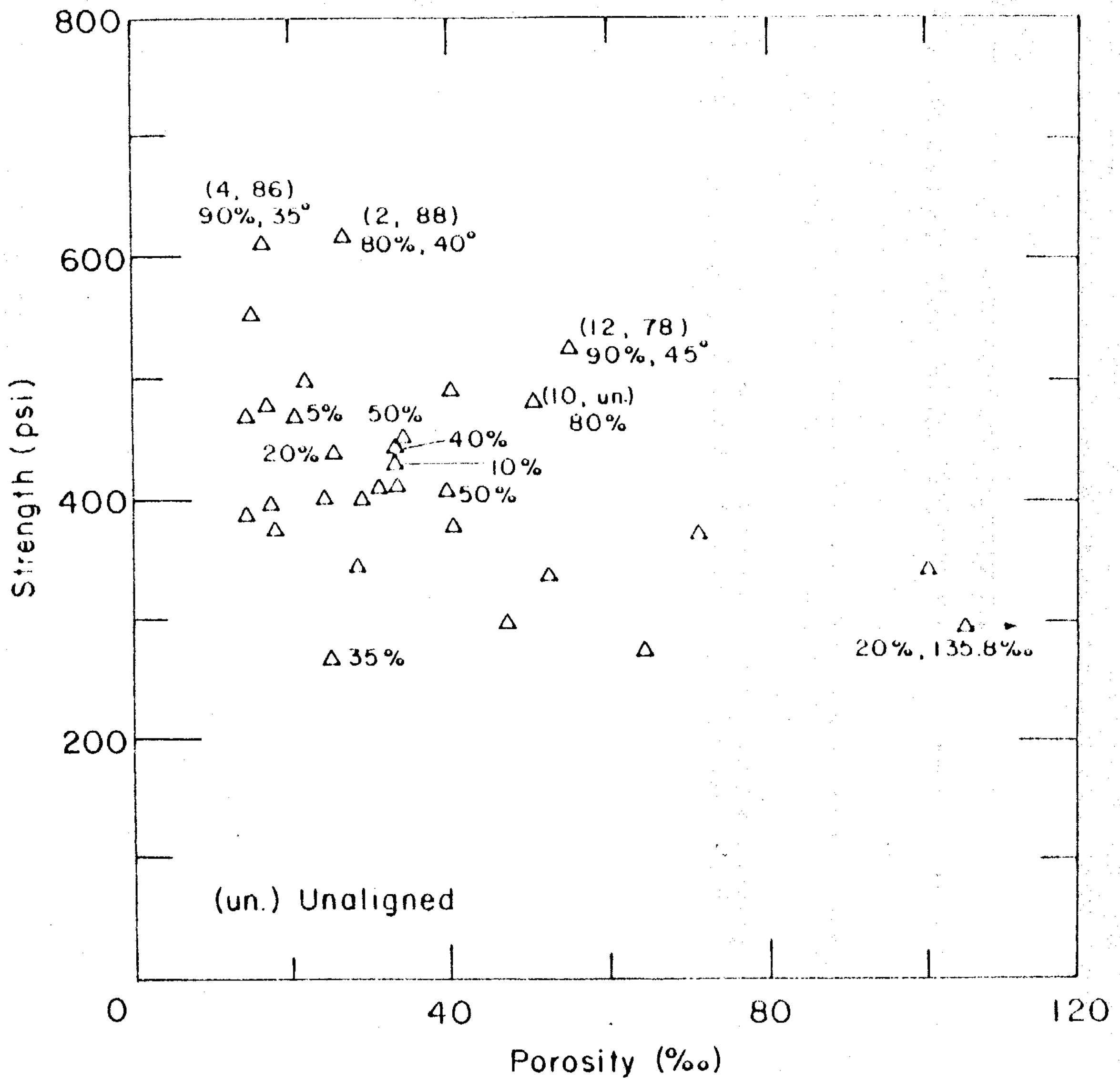

d. Tests conducted at 10^{-5} s^{-1} and −20°C.

interesting to study since these samples best represent the large-scale structural characteristics of the multi-year ridges. Ridges are also composed of fragments or blocks of columnar ice surrounded by a fine-grained matrix. As a result of our observations on mixed ice samples then, we would expect the columnar ice blocks incorporated into the ridge during its formation to influence the large-scale strength and deformation of the ridge. Since our study also indicates that many of these columnar blocks are preferentially oriented in a near horizontal position we anticipate a large-scale anisotropic behavior where the overall compressive strength of the ridge in the horizontal direction would be less than the vertical strength.

The porosity of the mixed and granular ice samples had a significant influence on their compressive strength at all test conditions. As the porosity of these samples increased, there was a decrease in strength at all test conditions.

The effect of grain size was considered in the evaluation of the columnar ice sample. Wang (1979) reported an increase in compressive strengh with a decrease in grain size for horizontally loaded, columnar first-year sea ice samples. We were unable to draw this same conclusion using our data set due to the wide variation in crystal orientation. Our results do indicate that the crystal orientation in columnar samples is the dominant characteristic influencing the compressive strength.

TESTED MULTI-YEAR FLOE ICE SAMPLES

During Phase I of the mechanical properties of multi-year sea ice program, techniques were developed to conduct uniaxial tension tests and conventional triaxial tests at constant loads. These tests were used extensively during the second phase of the test program. Multi-year ice samples from a presumably undeformed area were used to evaluate these techniques. There were a very limited number of tests done for each test type and condition. The results of these tests are discussed in the companion report by Cox et al. (1984) and the test techniques are presented in a second report by Mellor et al. (1984). The structural analysis of the multi-year floe samples is discussed in this report. The results of the structural analysis for each floe sample are presented in Appendix B.

In general, the influence of ice structure and crystal orientation on the strength of the multi-year floe samples is similar to that previously described for the ridge ice samples. Consequently, the following discussions are intentionally brief.

Ice Description

In general, the multi-year floe test samples had a columnar ice structure. A total of 58 floe samples were tested and of these samples 38, or 65%, were classified as columnar. The remainder of the samples consisted of mixed columnar and granular ice. A frequency histogram of the number of columnar floe samples in a given σ:z orientation is shown in Figure 9. The distribution of samples between σ:z = 0 and 90° and the presence of mixed ice samples suggests that the presumably undeformed sampling area on the floe was in fact part of the adjacent pressure ridge flank. In a truely undeformed area we would expect to see a higher percentage of columnar samples, all with an angle of σ:z near 0°.

A continuous structural profile of the ice in the sampling area is presented along with a detailed description in Cox et al. (1984).

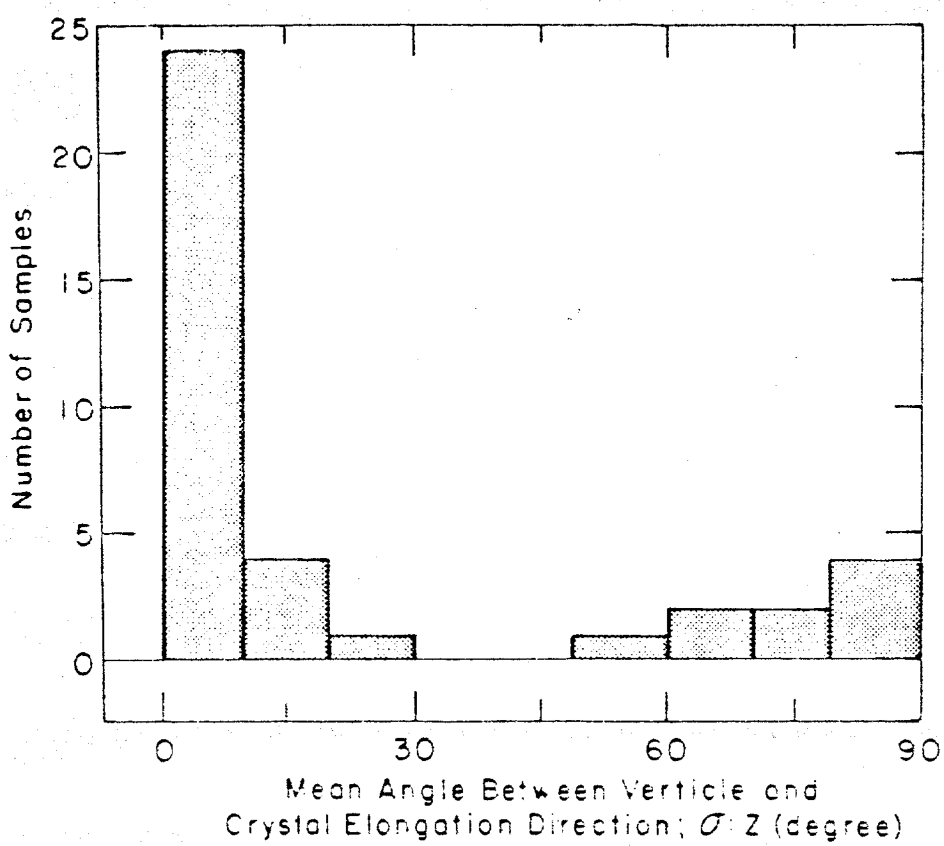

Figure 9. Frecuency histogram of the Phase I columnar floe ice samples in a given orientation.

Uniaxial constant-strain-rate compression tests

The compressive strength versus strain rate is plotted along with the structural classificaion of each test sample in Figure 10. The columnar samples at strain rates of 10^{-3} and 10^{-5} s^{-1} have also been plotted with the multi-year ridge ice samples results in Figure 7. In general, the compressive strengths of the multi-year floe samples agree well with those of the ridge samples when structural characteristics are taken into account.

Uniaxial constant-load compression tests

The structural classification of each test sample is indicated on a plot of strain rate minimum versus the applied stress in Figure 11. The influence of the c-axes orientation relative to the load (σ:z) is clearly evident at a stress of 600 psi. Those columnar samples with σ:z near 0° have a significantly lower strain-rate minimum than the samples with high σ:z angles. These results correlate with the results of the constant-strain-rate tests, supporting the correspondence between constant-load and and constant-strain-rate tests for ice suggested by Mellor (1980).

Uniaxial constant-strain-rate tension tests

The results from the tension tests are plotted in Figure 12. We have included the structural classification and crystallographic measurements for each sample in this figure. The tensile strength of the multi-year samples not only shows little variation with strain rate and temperature as discussed in Cox et al. (1984) and Cox and Richter-Menge (1985), it also shows little variation with c-axes orientation. This result is surprising since both Peyton (1966) and Dykins (1970) have noted a significant dependency on c-axes orientation in tension tests on first-year sea ice samples.

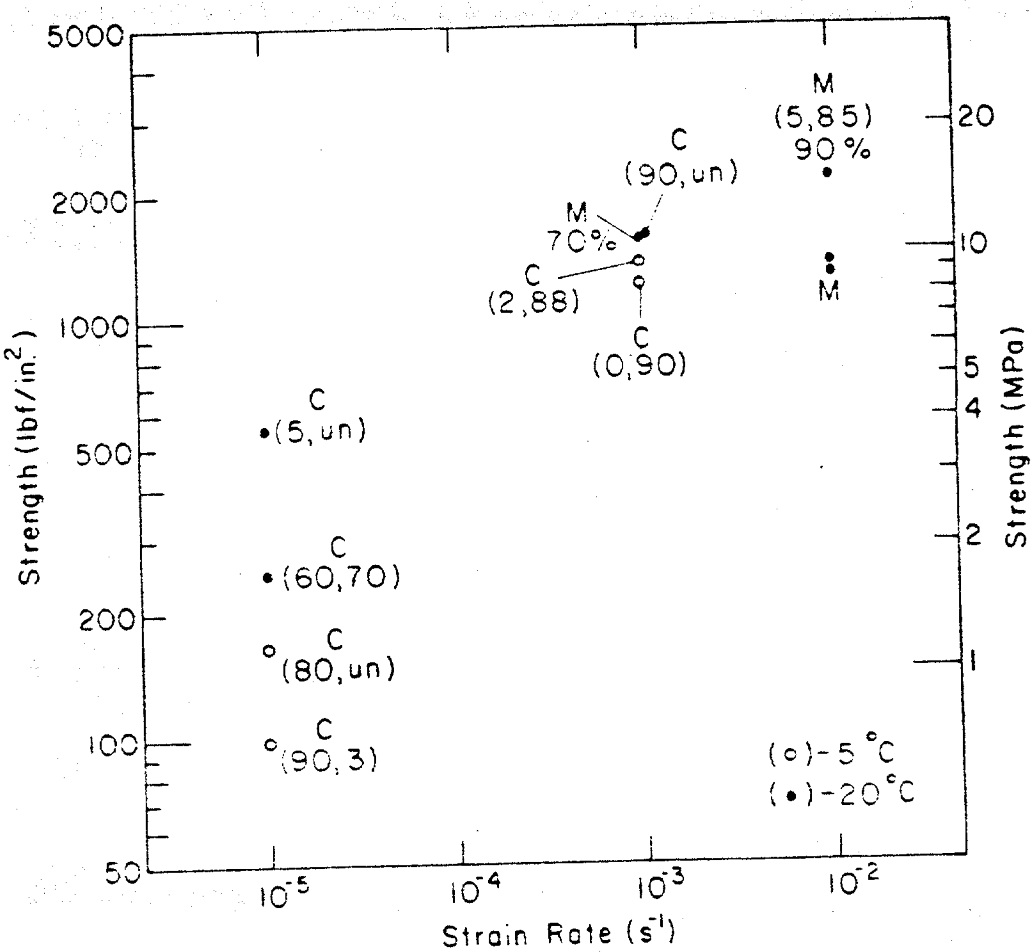

Figure 10. Uniaxial compressive strength of multi-year floe ice samples at -5 and -20°C versus strain rate. C = columnar ice and M = mixed granular and columnar ice. Crystallographic measurements indicated next to each sample: (c:z, c:c), % columnar.

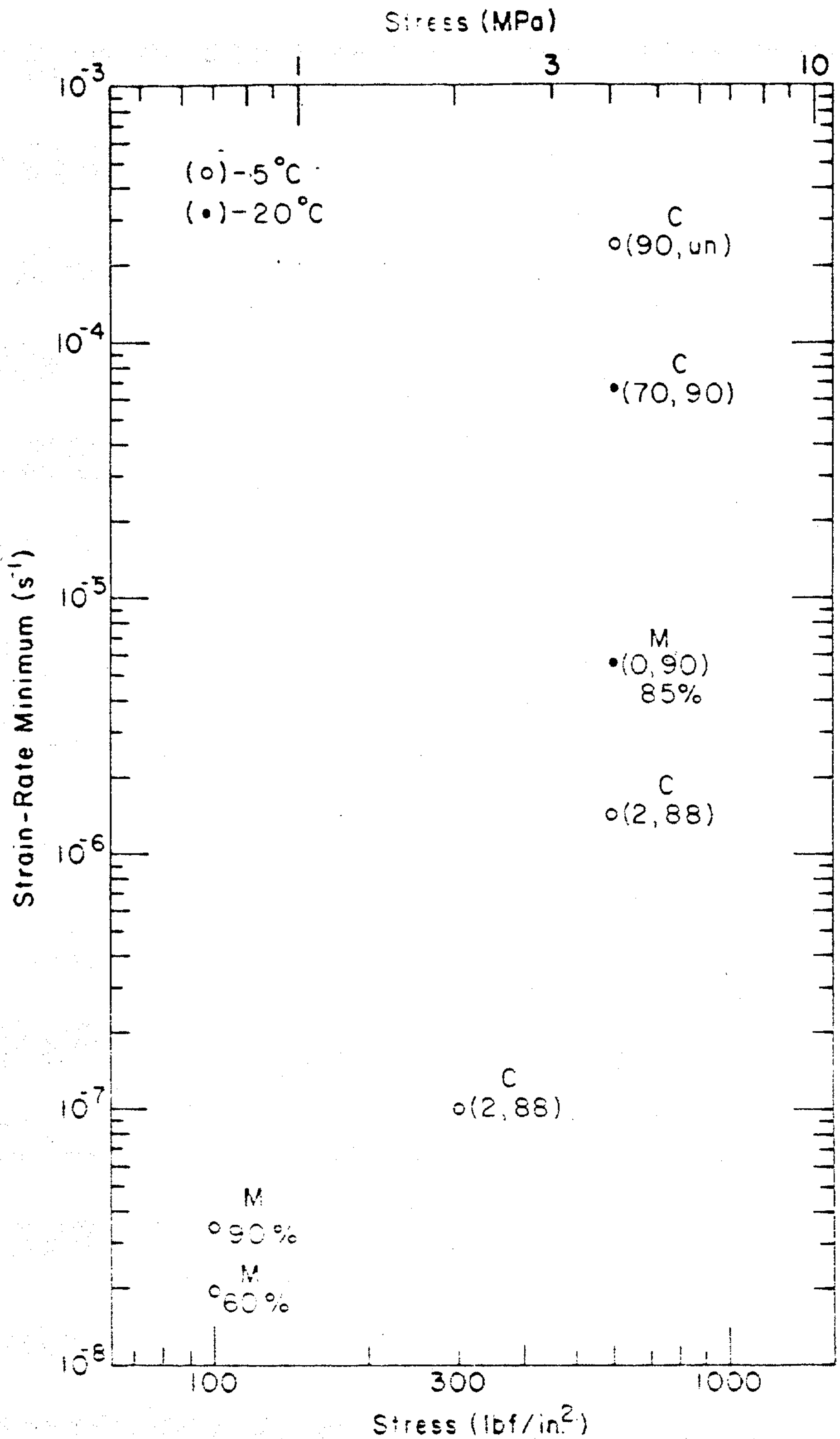

Figure 11. Strain-rate minimum versus applied stress for constant-load compression test results for the multi-year floe ice samples at -5 and -20°C. C = columnar ice and M = mixed granular and columnar ice. Crystallographic measurements indicated next to each sample: (c:z, c:c), % columnar.

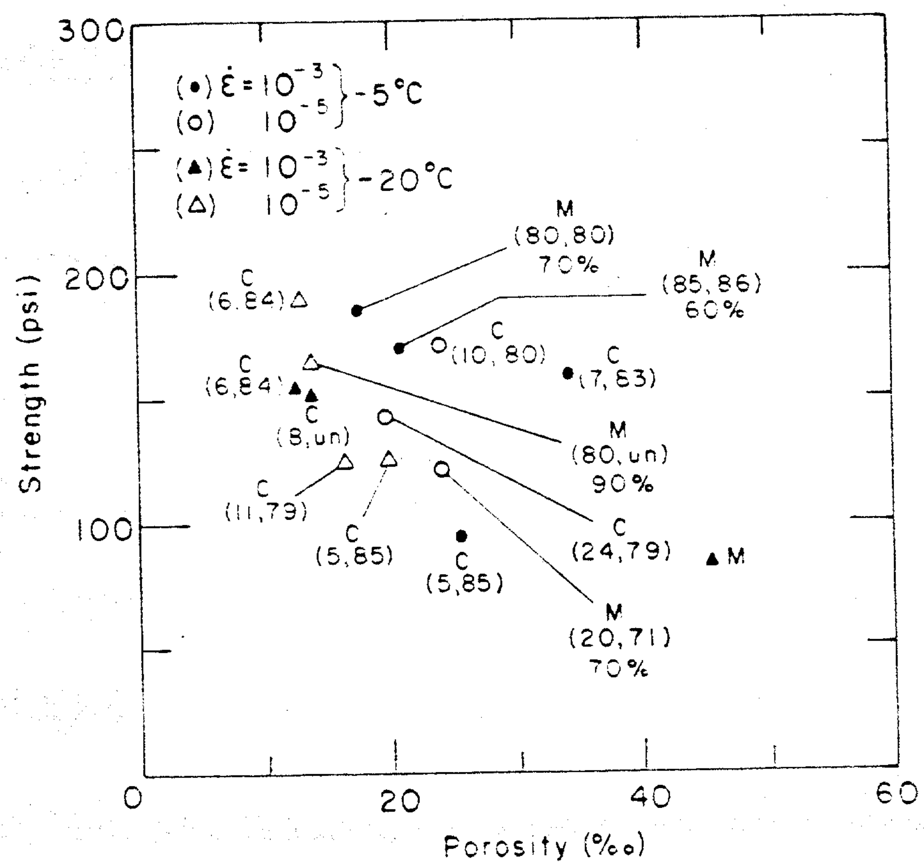

Figure 12. Uniaxial tensile strength of multi-year floe ice samples at -5 and -20°C. C = columnar ice and M = mixed granular and columnar ice. Crystallographic measurements indicated next to each sample: (c:z, c:c), % columnar.

Peyton's work shows that tensile samples with a σ:z angle of 0° can have a strength three times higher than a sample with σ:z = 90°. The strengths values of our samples do fall between those obtained by Dykins for vertical and horizontal first-year samples for a given porosity. The strength of the mixed ice samples was comparable to the strength of the columnar samples. In general, the multi-year tension tests indicate a decrease in strength with an increase in porosity. There did not appear to be a correlation between tensile strength and average grain size as observed in tensile tests on polycrystalline ice (Currier and Schulson, 1982).

All of the tension samples failed via an extension failure where the plane of failure was normal to the applied load. Location of the failure plane in the mixed ice samples coincided with a structural discontinuity.

Triaxial constant-strain-rate compression test

The triaxial tests that were performed in this program were conventional triaxial tests with $\sigma_1 > \sigma_2 = \sigma_3$ and σ_2/σ_1 = constant. The axial stress and radial stress is represented by σ_1 and σ_2, respectively. In general, the influence of c-axes orientation relative to the axial load was similar to that observed in the unconfined tests. Columnar samples with a σ:z angle near zero had high confined compressive strengths. The strength dropped off rapidly as σ:z increased. The influence of c-axes orientation was independent of temperature, strain-rate and confining ratio.

CONCLUSIONS

The internal structure of a multi-year ridge is extremely complicated and highly variable. The relative amounts of columnar and granular ice and their distribution within a ridge may vary depending on the original mode of formation of the ridges. Some ridges contain large blocks of columnar ice incorporated into the ridge during the compression of adjacent ice sheets. Other ridges, formed primarily by the shearing of one sheet against the other, are made up of highly fragmented ice. In a compression ridge, the columnar blocks appear to be in a near-horizontal position, as indicated by low angle measurements between the direction of elongation of the crystals and the vertical. The horizontally oriented, internal columnar ice blocks provide ice samples that exhibit anisotropic behavior under loading. For instance, if a vertically cored columnar sample is taken from such an ice block and is loaded vertically its compressive strength may be 2-3 times higher than if the sample had been cored and loaded horizontally. Based on this observation then, we would expect the mean compressive strength obtained from a series of tests on vertical ridge samples to be higher than the mean value obtained from horizontal samples. The variation would be dependent on the number of columnar ice blocks and their orientation within a ridge. In addition, the presence of preferentially oriented columnar ice blocks may also affect the large-scale mechanical properties of the multi-year pressure ridge. If the ridge contains a significant number of large columnar blocks of ice in which the direction of crystal elongation is near vertical we might expect anisotropic behavior. In this case the overall strength of the ridge would be higher if loaded in the vertical direction.

All of this points to the fact that interpretation of multi-year ridge data is incomplete without a thorough structural analysis of the samples tested. Based on the first phase of our study we can make the following general conclusions concerning the influence of ice structure on the compressive strength of multi-year ridge ice samples:

- For columnar ice samples, the dominant characteristic that influences sample strength is crystal orientation. Columnar samples with the direction of crystal elongation near vertical and with a high degree of crystal c-axes alignment will have extremely high compressive strengths. When the direction of crystal elongation coincides with the direction of maximum shear at an angle of 45° to the load, the columnar samples have a very low compressive strength.
- A sample composed of both columnar and granular ice (classified as a mixed ice sample) will exhibit the same mechanical properties as a columnar sample if it contains greater than or equal to 80% columnar ice.
- The orientation of the columnar fragments in a mixed ice sample influence the overall compressive strength and deformational characteristics of the sample. If the columnar fragments are oriented in a hard fail direction the sample will have a relatively high strength. Failure in these samples will occur in the granular material surrounding the columnar fragments.
- Mixed and granular ice samples show a significant decrease in strength with an increase in ice porosity.

REFERENCES

Cherepanov, N.V. (1974) Classification of ice of natural water bodies. Proceedings of the IEEE International Conference on Engineering in the Ocean Environment, OCEAN '74, Halifax, Nova Scotia, vol. 1, 21-23 August 1974, pp. 97-101.

Cox, G.F.N., J.A. Richter-Menge, W.F. Weeks, M. Mellor, H.W. Bosworth, G. Durell and N. Perron (in press) Mechanical properties of multi-year sea ice, Phase II: Test results. U.S. Army Cold Regions Research and Engineering Laboratory, report in press.

Cox, G.F.N. and J.A. Richter-Menge (1985) Tensile strength of multi-year pressure ridge sea ice samples. Proceedings of the Fourth International Offshore Mechanics and Arctic Engineering Symposium, Dallas, TX, February, 1985.

Cox, G.F.N., J.A. Richter-Menge, W.F. Weeks, M. Mellor and H. Bosworth (1984) Mechanical properties of multi-year sea ice, Phase I: Test results. U.S. Army Cold Regions Research and Engineering Laboratory, CRREL Report 84-9.

Cox, G.F.N. and W.F. Weeks (1983) Equations for determining the gas and brine volumes in sea ice samples. Journal of Glaciology, vol. 29, no. 102, pp. 306-316.

Currier, J.H. and E.M. Schulson (1982) The tensile strength of ice as a function of grain size. Acta Metallurgica, vol. 30, pp. 1511-1514.

Dykins, J.E. (1970) Ice Engineering: Tensile properties of sea ice grown in a confined system. Naval Civil Engineering Laboratory, Technical Report R689, 56 p.

Jaeger, J.C. and N.G.W. Cook (1969) Fundamentals of Rock Mechanics. Methuen and Co., Ltd., London, England.

Kovacs, A. and M. Mellor (1974) Sea ice morphology and ice as a geological agent in the southern Beaufort Sea. The coast and shelf of the Beaufort Sea, Proceedings of the Arctic Institute of North America, Symposium on Beaufort Sea Coast and Shelf Research.

Langway, C.C. (1958) Ice fabrics and the universal stage. SIPRE Technical Report 62.

Mellor, M., G.F.N. Cox and H.W. Bosworth (1984) Mechanical properties of multi-year sea ice: Testing techniques. U.S. Army Cold Regions Research and Engineering Laboratory, CRREL Report 84-8.

Mellor, M. (1980) Mechanical properties of polycrystalline ice. Physics and Mechanics of Ice, Proceedings of the International Union of Theoretical and Applied Mechanics Symposium, Copenhagen, 6-10 August 1979. New York: Springer-Verlag, pp. 217-245.

Michel, B. (1978) Ice Mechanics. Les Presses de L'Université Laval, Quebec, Canada.

Peyton, H.R. (1966) Sea ice strength. Geophysical Institute, University of Alaska, Report UAG-182.

Richter-Menge, J.A., G.F.N. Cox, N. Perron, G. Durell and H.W. Bosworth (in prep.) Triaxial testing of first-year sea ice. U.S. Army Cold Regions Research and Engineering Laboratory. Internal Report 877.

Richter-Menge, J.A. and G.F.N. Cox (1985) The effect of sample orientation on the compressive strength of multi-year pressure ridge ice samples. Proceedings of the Conference Arctic '85, ASCE, San Francisco, Ca., 25-27 March 1985, pp. 465-475.

Tucker, W.B. III, A.J. Gow and W.F. Weeks (1985) Physical properties of sea ice in the Greenland Sea. Proceedings of the Eighth International Conference on Port and Ocean Engineering Under Arctic Conditions, Narssarssuaq, Greenland, 6-13 September 1985.

Wang, W.S. (1979) Crystallographic studies and strength tests of field ice in the Alaskan Beaufort Sea. Proceedings of the Fifth International Conference on Port and Ocean Engineering Under Arctic Conditions, Trondheim, Norway, vol. 1, pp. 651-665.

Weeks, W.F. and A.J. Gow (1978) Preferred crystal orientation in the fast ice along the margins of the Arctic Ocean. Journal of Geophysical Research, vol. 83, no. C10, pp. 5105-5121.

APPENDIX A. MULTI-YEAR RIDGE SAMPLES DATA.

This appendix contains the results from the structural analysis of the constant-strain-rate uniaxial compression tests performed on multi-year ridge ice samples. The parameters listed for each test are defined in Index A. STR.A-3-5 denotes the structural analysis of the above-level-ice samples tested in uniaxial compression at a strain rate of 10^{-3} s^{-1} and a temperature of -5°C, etc. B indicates samples that were taken below level ice. The sample number R1A-175/201 gives the location and depth of the sample; that is, Ridge 1, hole A, at a depth of 175 to 201 cm. All of these samples were vertically cored.

INDEX A

Column Number	Symbol	Description
1	σ_m (psi)	Peak stress or strength
2	ε_m (GL) (%)	Strain at σ_m determined by the DCDTs over a gauge length of 5.5 in.
3	t_m (s)	Time to peak stress
4	E_i (GL) (10^6 psi)	Initial tangent modulus determined using strains found over the gauge length
5	t_e (s)	Time to end of test
6	σ_e/σ_m	Ratio of end to peak stress at 5% full sample strain
7	$n(o/_{oo})$	Samples porosity at test temperature
8	Classification	Classification of ice texture type as granular (1), columnar (2) or a mixture of granular and columnar (3)
9	Subgroup	Subgroup classification
10	% columnar	Estimation of % columnar ice in the sample
11 12 13	min (mm) max (mm mean (mm)	Measurement of the minimum, maximum and mean columnar grain size as measured across the width of the grain
14	σ:z (degree)	Angle between the direction of crystal elongation and the vertical
15	σ:c	Angle between the vertical load and the mean crystal c-axes direction
16	Spread (degree)	Degree of alignment of the c-axes. U, A and R represent unaligned, aligned and random, respectively.
17 18 19	min (mm) max (mm) mean (mm)	Measurement of the minimum, maximum and mean granular grain size
20	Type failure	Dominant failure mode. L = longitudinal splittings, S = shear, and MS = multiple shear failure
21	Location	Location of failed area in sample. T = top, M = middle, and B = bottom of sample

FILE STR.A-3-5

SAMPLE #	01	02	03	04	05	06	07	08	09	10	11	12	13	14	15	16	17	18	19	20	21
R1A-175/201	1270	.140	1.45	1.200	50.0	.094	16.2	2	A	100	2	15	8	10	85	30					
R1B-131/157	1260	.160	2.35	1.320	50.0	.166	12.3	3		95			8	16		U			1.0	L	M
R2A-110/135	408	.050	.44	.868	.4		86.9	1											2.0	L	M
R2B-135/161	820	.110	1.00	.892	1.0		26.8	1											2.0	L	M-B
R3A-188/213	970	.160	1.64	1.060	50.0	.205	23.5	3												MS	M
R3B-130/155	900	.140	1.50	1.170	50.0	.283	30.3	3		95			10	68	30	60			1.0	MS	M
R4A-283/309	860	.110	1.00	.973	1.0		78.7	3												L	M
R4B-299/325	910	.140	1.50	.973	50.0	.109	56.2	3												MS	M
R5A-135/161	1090	.100	.85	1.220	.8		22.9	2	C										7.0	L	M
R5B-141/167	1270	.110	1.30	1.280	1.3		21.1	2	C					2	90	30				L	M
R7A-005/031	731	.090	1.08	.781	1.1		76.4	1									1	6	2.0	L	M
R7B-072/098	487	.060	1.40	2.030	1.4		53.4	3		20			10				0	5	1.0	L	M
R8A-033/059	346	.060	1.15	.718	1.1		75.2	3	A	70			7	16	76	50	1	4	3.0	L	T
R8B-011/037	811	.090	.80	.997	.8		84.9	3		70										L	M
R2C-049/076	642	.110	1.15	.806	50.0	.217	132.1	3	B											MS	T
R2D-134/161	706	.120	1.70	.821	50.0	.197	84.8	3	B											MS	B
R4C-244/271	760	.070	1.08	1.140	1.1		49.2	2	A	100	4	12	10	14	78	60				L	T-M
R4C-309/336	826	.160	2.17	.897	50.0	.226	42.1	3		10									1.0	MS	M
R4D-228/255	656	.060	.95	1.110	.9		52.3	2	A	95	5	15	10	10	80	90				L	M
R7C-007/034	907	.120	1.12	.941	1.1		53.8	3												S	M
R6A-398/425	764	.130	1.45	.880	50.0	.120	98.3	3												MS	B
R6A-504/531	824	.160	2.03	.952	50.0	.261	75.3	3	B											MS	M
R7D-088/114	1007	.180	1.69	.875	50.0	.194	41.2	3												MS	M
R9C-080/107	879	.150	1.87	.973	50.0	.267	50.4	3	B											MS	B
R9D-082/109	816	.150	1.69	.875	50.0	.103	66.7	3												MS	M

FILE STR.B-3-5

SAMPLE #	01	02	03	04	05	06	07	08	09	10	11	12	13	14	15	16	17	18	19	20	21
R1A-300/326	1580	.120	1.38	1.430	1.4		20.3	2	A	100	2	20	12	6	85	40				L	M
R1B-216/241	915	.120	1.70	1.250	50.0	.213	16.3	2		100	3	20	12	45		U				MS	M
R1B-243/268	1050	.150	1.40	1.250	50.0	.136	20.4	2	A	100	4	17	10	30		U				MS	M
R2A-285/310	1270	.160	2.20	1.180	50.0	.075	22.3	3		80	5	18	10	12	70	A	0	5	3.0	MS	M
R2A-383/408	1060	.110	1.10	1.300	1.1		31.1	2	A	95	2	15	10	35		U	0	5	1.0	L	M
R2B-351/377	1130	.140	1.26	1.150	1.3		43.8	3	A	90	5	20	15	18		U			1.0	L	T-M
R2B-438/464	995	.140	1.80	1.020	50.0	.150	44.6	3												MS	T-M
R3A-401/427	925	.160	1.52	1.050	50.0	.177	21.0	3	B	40			7						1.0	MS	M-B
R3B-239/265	870	.160	1.60	.997	50.0	.293	25.6	3												MS	M
R3B-331/357	971	.160	1.75	1.050	50.0	.217	31.4	3	B	5									1.0	MS	M
R4A-398/423	786	.140	2.10	.997	50.0	.183	36.5	3	B											MS	M
R4B-358/384	776	.120	1.68	.892	50.0	.128	44.4	3	B											MS	T-M
R4B-420/446	910	.150	1.85	1.060	1.8		53.0	2	A		2	17	8	8	82	55				S	M
R5A-473/499	875	.140	1.68	.949	50.0	.193	37.1	3	B	10							0	10	1.0	MS	T-M
R5B-287/313	1040	.100	1.05	1.310	1.0		51.4	2			5	25	15			U				L	M
R5B-370/396	816	.120	1.40	.989	50.0	.183	52.3	3												MS	M
R7A-232/258	736	.120	1.83	.908	50.0	.182	165.3	3		80				30	65	A				MS	T-M
R7A-295/321	612	.110	2.08	.900	2.3		66.1	1									0	3		L	M-B
R7B-175/201	557	.060	.43	.876	.4		23.3	1									1	15	5.0	S	T
R7B-440/466	1540	.170	2.30	1.250	2.3		32.0	2	A	100	2	20	7	5	85	35				L	M
R8A-305/331	589	.110	1.05	.728	50.0	.413	27.2	3												MS	M
R8A-384/410	1297	.150	1.69	1.270	1.7		24.2	2	A		4	15	8	26	70	A				S	M-B
R8B-300/326	587	.170	2.93	1.170	50.0	.421	15.1	3	B											MS	M
R8B-483/508	1440	.200	3.78	1.140	3.8		25.6	2	A		5	15	8	12	78	50				L	B
R2C-196/223	844	.150	1.40	.899	50.0	.188	45.3	3	B	30									1.0	MS	M
R2C-278/305	674	.140	1.93		50.0	.341	71.5	3	B	25									1.0	MS	M-B
R2D-220/247	760	.120	1.49	.900	1.5		50.1	3	B										2.0	S	M

FILE STR.B-3-5 (Continued)

R2D-344/371	732	.130	1.70	.842	50.0	.157	68.1	3		70	5	12		U	1.0	MS	M
R4C-414/441	716	.160	1.62	.905	50.0	.267	43.7	2	A	100	10	26	68	110		MS	M
R4C-512/539	816	.130	1.54	.903	50.0	.074	36.6	3								S	M
R4D-495/522	617	.110	1.57	1.030	33.6		35.7	2	A	100		20				S	M
R6C-476/503	852	.170	1.87	.834	50.0	.177	59.9	3								MS	M
R7C-143/170	1015	.160	2.23	.962	50.0	.247	26.4	3								MS	M
R7C-541/568	975	.170	1.55	.951	50.0	.155	22.5	3								MS	M
R7D-223/250	923	.200	2.41	.875	50.0	.224	54.0	3								MS	T-M
R7D-312/339	963	.170	1.76	.907	50.0	.219	55.3	3								MS	M
R9A-445/482	637	.130	1.85	.814	50.0	.104	68.6	3								MS	M
R9B-329/356	804	.090	1.06	1.000	1.1		48.4	3								L	M
R9C-332/359	676	.140	2.06	.875	50.0	.184	49.3	3								MS	T-M
R9D-249/276	728	.140	1.82	.921	50.0	.104	71.1	3								MS	M-B
R10A-269/296	971	.180	1.84	.984	50.0	.283	24.8	3								MS	M
R10B-274/301	955	.170	1.81	1.060	50.0	.259	27.1	3								MS	B
R10C-445/472	828	.110	1.30	1.190	1.3		32.7	2	A			10	82	80		S	T
R10D-231/258	903	.170	1.77	.936	50.0	.145	23.5	3								L	T

FILE STR.A-5-5

SAMPLE #	01	02	03	04	05	06	07	08	09	10	11	12	13	14	15	16	17	18	19	20	21
R1A-062/089	443	.310	344.00	1.660	5000.0	.528	59.0	1											3.0	MS	B
R1B-062/089	328	.110	365.00	.973	5000.0	.652	51.3	1									0	5	3.0	MS	T-M
R2A-140/165	388	.660	683.00	.804	5000.0	.655	10.1	1									0	5	3.0	MS	M
R2B-094/121	171	.110	156.00	.563	5000.0	1.029	143.0	3	B	75				24	78	30			1.0	S	M
R3A-106/131	342	.460	855.00	.654	5000.0	.734	35.9	1											4.0	MS	M
R3B-161/187	308	.360	360.00	.598	5000.0	.672	19.2	1									1	7	4.0	S	M
R4A-312/338	283	.470	465.00	.703	5000.0	.682	76.1	3		5							0	5	1.0	MS	M
R4B-328/354	253	.400	615.00	.411	5000.0	.656	38.1	3		10							1	8	3.0	MS	M
R5A-165/191	619	.240	217.00	1.500	5000.0	.443	16.9	3		80	1	8	4	10	80	30			1.0	S	M
R5B-075/101	774	.190	201.00	1.180	5000.0	.318	72.3	3		90	2	10	7	5	85	60			1.0	S	T
R7A-059/085	361	.470	588.00	.804	5000.0	.701	69.5	1									0	3	1.0	MS	M
R7B-126/152	240	.490	468.00	.603	5000.0	.863	98.2	3		5							0	7	3.0	S	M
R8A-133/159	245	.340	333.00	.675	5000.0	.849	34.5	3												MS	M-B
R8B-162/189	336	.370	473.00	.560	5000.0	.699	25.4	3	B										1.0	MS	M
R3C-095/122	268	.400	472.00	.524	5000.0	.765	48.0	3	B											MS	T
R3D-159/186	201	.750	700.00	.578	5000.0		140.5	3	B	20									1.0	MS	T
R5C-039/066	376	.470	416.00	.875	5000.0	.678	86.6	3	B	25									1.0	MS	M
R5D-159/186	384	.560	690.00	.438	5000.0	.667	26.3	3												MS	B
R6C-166/193	210	.280	300.00	.661	5000.0	1.062	118.8	3	B	50				18	76	70				MS	B
R8C-048/075	239	.310	278.00	.637	5000.0	.753	58.6	3	B											MS	B
R8D-236/263	331	.160	248.00	.910	5000.0	.804	49.8	3	B	80										MS	T
R10C-063/090	306	.470	444.00	.778	5000.0	.771	27.5	3												MS	M
R10D-126/153	301	.500	484.00	.770	5000.0	.714	38.1	3												MS	T

FILE STR.R-5-5

SAMPLE #	01	02	03	04	05	06	07	08	09	10	11	12	13	14	15	16	17	18	19	20	21
R1A-226/252	214	.210	173.00	.916	5000.0	.579	19.4	2	A	100				22	68	45				S	T-M
R1A-399/425	214	.290	248.00	.751	5000.0	.696	38.9	3	B	50			10				0	10	1.0	MS	T-M
R1B-320/346	1090	.300	253.00	1.010	5000.0	.173	25.3	2	A	100	5	25	10	2	88	50					
R1B-429/455	696	.270	285.00	1.150	5000.0	.386	23.7	2	A	90	3	15	10	10		U			1.0	MS	T
R2A-205/230	443	.390	489.00	.892	2975.0		38.6	3									1	8	2.0	MS	MS
R2A-314/339	308	.250	278.00	.667	5000.0	.523	32.5	2	A	100	5	15	10	30	68	90				S	M
R2B-408/434	342	.570	597.00	.662	5000.0	.763	34.6	3		5							0	5	1.0	MS	B
R2B-468/494	265	.420	390.00	1.070	5000.0	.751	32.0	3		10									1.0	MS	M
R3A-220/245	253	.270	387.00	.350	5000.0	.731	22.3	3		35			8						1.0	MS	T
R3A-430/456	306	.410	525.00	.782	5000.0	.703	43.3	3	B	35	3	15							1.0	MS	B
R3B-363/389	394	.510	507.00	.787	5000.0	.657	15.3	3	B	5							0	8	1.0	MS	M-B
R4A-426/452	322	.270	330.00	.782	5000.0	.568	40.8	3	B	30	2	15	7				0	5	1.0	S	T
R4B-391/417	290	.300	308.00	.751	5000.0	.638	40.8	3	B	10			10				0	3	1.0	MS	M
R4B-449/475	243	.420	368.00	.521	5000.0	.720	34.2	3												MS	M
R5A-397/423	314	.360	558.00	.420	5000.0	.723	23.8	3		5							0	10	1.0	S	B
R5A-442/468	462	.290	279.00	1.000	5000.0	.472	22.1	3												S	T
R5A-504/530	327	.450	555.00	.395	5000.0	.694	28.1	3									0	10	1.0	MS	M
R5B-341/367	368	.610	608.00	.804	5000.0	.717	56.1	1									1	4	2.0		
R5B-398/423	300	.400	525.00	.609	5000.0	.770	28.7	3												MS	M-B
R7A-263/289	68	.060	96.00	.425	5000.0	.897	153.9	2	A	100	7	25	15	50	55	20				S	M-B
R7A-342/368	607	.160	255.00	.908	5000.0	.321	24.4	2	C	100	2	20		20		U				L	T
R7B-241/267	229	.340	465.00	.523	5000.0	.712	77.8	3		5							3	10	5.0	MS	T
R7B-410/436								2	A	100			10			A				S	M
R8A-164/190	261	.110	285.00	.536	5000.0	.670	28.1	3	A	80			5						1.0	S	M
R8A-432/458	657	.160	156.00	1.070	5000.0	.317	24.5	2	A	100	2	15	8	10	80	40				S	M
R8B-333/359	344	.250	248.00	.479	5000.0	.608	21.4	3												MS	M-B

FILE STR.B-5-5 (Continued)

R8B-515/541	348	.400		.592	5000.0		23.8	3		40	3	12	7	20	76	50			1.0	MS	T-M
R3C-296/323	286	.680	650.00	.549	1250.0		42.2	3												MS	T
R3C-380/407	189	.110	188.00	.554	5000.0	.693	48.3	2	A		5	20		35						S	M
R3D-219/246	269	.330	380.00	.628	5000.0	.993	81.1	3									0	10		MS	T
R3D-287/314	334	.620	710.00	.698	5000.0	.749	36.8	3	B	10									1.0	MS	M
R5C-219/246	314	.510	550.00	.467	5000.0	.710	42.6	3						90						S	B
R5C-282/309	279	.510	520.00	.504	5000.0	.742	61.0	3												MS	M
R5D-225/252	382	.450	480.00	.603	5000.0	.641	31.8	3												MS	M
R5D-294/321	337	.420	548.00	1.090	5000.0	.902	29.6	3												MS	M
R6A-562/589	223	.590	538.00	.634	5000.0	.771	83.1	3	B											MS	T-M
R6C-529/556	368	.830	777.00	.834	5000.0	.731	29.7	3												MS	B
R8C-378/405	762	.170	245.00	1.430	5000.0	.286	25.4	2	A	100	2	15	10	6	85	40				S	M
R8C-476/503	148	.320	257.00	.648	5000.0	.655	22.9	2	A	100	2	12	8	30	72	45				S	M
R8D-446/473	226	.170	237.00	.654	5000.0	.916	33.8	2						5	85	90				S	M
R8D-543/561	240	.220	210.00	.648	5000.0	.517	30.8	2						30		U				MS	T-M
R9A-341/368	276	.480	488.00	.700	5000.0	.743	69.5	3											2.0	MS	T
R9B-385/412	287	.770	704.00	.609	5000.0	.808	54.0	3	B										2.0	MS	M
R9C-426/453	283	.480	459.00	.737	5000.0	.781	29.2	3											3.0	MS	M-B
R9D-181/208	255	.290	291.00	1.050	5000.0	.820	26.6	3												S	T
R10A-351/378	369	.770	721.00	.722	5000.0	.743	12.4	3	B										.5	MS	M-B
R10B-351/378	331	.370	439.00	.824	5000.0	.731	17.8	2	A	100	2	10	6	15	75	20				S	T
R10C-316/343	272	.290	309.00	.599	5000.0	.750	45.2	3					5	20		U				MS	B
R10D-325/352	365	.280	340.00	.693	5000.0	.603	30.9	3												MS	T

FILE STR.A-3-20

SAMPLE #	01	02	03	04	05	06	07	08	09	10	11	12	13	14	15	16	17	18	19	20	21
R1C-127/154	1520	.150	1.66	1.400	1.7		23.8	3		10			7				1	15	5.0		
R1D-153/178	1270	.100	.84	1.520	.8		25.4													S	T-M
R2C-129/156	1580	.180	2.45	.709	2.4		52.5	3												S	M
R2D-095/122	1230	.170	1.54	.951	1.5		73.9	3	B	25									1.0	S	M
R4D-198/225	1140	.110	1.30		1.3		56.5	2	A	100	3	15	5	12	80	50				S	M
R6A-531/558	1200	.200	1.75	.957	50.0	.169	58.1	3												MS	B
R6C-134/161	1320	.180	1.74	.973	1.7		87.1	3	B											S	M
R7C-092/119	1760	.050	2.60	1.090	16.5		30.1	3													
R7D-036/063	1720	.230	2.45	1.090	2.4		40.1	3		5							0	5	2.0	L	T
R9A-071/098	1237	.200	2.35	.941	2.6		113.1	3												S	M
R9B-076/103	1110	.200	2.45	1.000	50.0	.047	117.4	1												S	M
R9C-049/076	1480	.230	2.76	1.170	50.0	.164	47.0	3												MS	M
R9D-150/177	1530	.250	2.55	1.090	50.0	.135	35.4	2					5	40		U				MS	T
R10A-238/265	1838	.220	3.33	1.270	4.3		18.0	2			3	20	10	30	62	95				L	M
R10B-084/111	1510	.210	2.28	1.170	50.0	.113	21.5	3												MS	M

FILE STR.B-3-20

SAMPLE #	01	02	03	04	05	06	07	08	09	10	11	12	13	14	15	16	17	18	19	20	21
R1C-349/375	1440	.190	1.80	1.310	1.8		27.0	3	B											L	M
R1C-384/410	1020	.110	1.02	1.100	1.0		56.2	3	B	60										L	M
R1D-179/206	1640	.140	1.84	1.450	1.8		18.1	2	A	100	2	20	8	18	82	30				L	M
R1D-285/312	1650	.110		1.570			12.9	2	A	100	3	15	10	10	82	30				L	M
R2C-226/253	1480	.200	2.64	1.080	50.0	.080	49.3	3												S	M
R2C-310/337	1070	.200	3.36	.904	17.6		50.5	3		10			3						1.0	L	T-M
R2D-265/292	1410	.170	2.28	1.030	2.3		50.3	3		60	2	15	7	5	85	40	0	10	5.0	S	M
R2D-406/433	1100	.200	2.72	.933	50.0	.101	45.5	3					5						1.0	S	T-M
R4C-482/509	1420	.220	2.40	1.070	50.0	.197	31.5	3												MS	M
R4C-543/570	1400	.210	2.84	1.090	42.2		29.8	3											2.0	MS	M-B
R4D-382/409	1430	.220	2.92	1.080	50.0	.170	21.8	3	B		2	15	10	5	85	40				MS	M
R4D-414/441	1310	.160	1.48	1.030	1.5		41.5	3	B											S	M
R4D-525/552	1300	.200	2.70	1.050	2.7		25.1	3		65	5	20	10	24	66	30			3.0	S	T
R6C-559/586	1440	.240	2.60	.995	50.0	.157	33.3	3											2.0	MS	M
R7C-457/484	1650	.240	3.17	1.170	50.0	.746	12.3	3												MS	M
R7C-572/599	1760	.230	2.85	1.210	2.8		17.7	3												L	M
R7D-254/281	1310	.230	3.14	1.000	50.0	.276	36.4	3									0			MS	M
R7D-546/573	1480	.230	2.70	.889	50.0	.164	16.8	3												MS	M
R9A-424/451	1120	.160	1.68	.898	1.7		62.3	3		5			5				0	5	1.0	S	M
R9B-417/444	1400	.200	2.70	.973	2.7		55.6	3												S	M
R9C-507/534	1340	.210	2.16	1.170	50.0	.211	19.3	3											3.0	MS	M
R9D-348/375	1150	.130	1.52	1.150	1.5		40.1	3											2.0	S	M
R10A-407/434	1480	.210	2.87	1.180	50.0	.245	13.8	3												MS	M
R10B-449/476	1470	.170	2.53	1.230	50.0	.190	14.0	2						20		U				MS	M
R10C-506/533	1230	.200	2.53	1.160	50.0	.181	22.7	2						12	78	70				MS	B
R10D-508/535	1310	.190	2.26	1.140	50.0	.155	17.4	2												MS	B

FILE STR.A-5-20

SAMPLE #	01	02	03	04	05	06	07	08	09	10	11	12	13	14	15	16	17	18	19	20	21
R1C-065/092	617	.170	192.00	1.520	5000.0	.371	26.8	3		80			10	2	88	40	0	4	1.0		
R1D-071/098	612	.220	219.00	1.000	5000.0	.315	16.6	3	A	90	2	15	10	4	86	35				S	M
R3C-128/155	436	.350	341.00	.847	5000.0	.711	25.6	3		20			10				0	5	1.0	MS	T
R3D-129/156	289	.220	269.00	.682	5000.0	.830	135.8	3		20							0	10	1.0	S	T
R5C-097/124	368	.260	373.00	.800	3830.0		71.4	3									1	10	3.0		
R5D-121/148	342	.180	240.00	1.050	5000.0	.851	28.5	3									1	10	3.0	MS	B
R6A-461/488	330	.270	278.00	.745	5000.0	.906	52.2	3									2	15	5.0	MS	M
R8C-165/192	522	.270	334.00	1.080	5000.0	.628	55.5	3	A	90			8	12	78	45			1.0	S	T-M
R8D-192/219	476	.220	253.00	.898	5000.0	.632	50.4	3	B	80	1	7	15	10		U			1.0	S	B
R9A-125/152	361	.430	449.00	.875	5000.0	.970	112.6	3												S	T
R9B-043/070	337	.450	447.00	.875	5000.0	.911	100.5	3												S	M
R10A-195/222	330	.220	264.00	.810	5000.0	.715	23.4	1								R	2	20	10.0	MS	M
R10B-243/270	525	.100	154.00	1.120	5000.0	.389	20.9	2			2	20	10	30	62	100				S	M
R10C-032/059	484	.730	696.00	.707	5000.0	.818	40.1	3											1.0	MS	M-B
R10D-157/184	390	.420	468.00	.928	5000.0	.772	14.4	3	B											MS	B

FILE STR.B-5-20

SAMPLE #	01	02	03	04	05	06	07	08	09	10	11	12	13	14	15	16	17	18	19	20	21
R1C-210/236	403	.220	282.00	.769	5000.0	.593	39.7	3	B	50	5	20	15				0	2	1.0	S	T
R1C-240/266	443	.250	246.00	.989	5000.0	.558	33.3	3	B	40	2	20	10				0	1	.5	S	M
R1D-209/236	557	.170	282.00	.876	5000.0	.456	28.6	2	A	100	2	20	15	14		U				S	T
R1D-315/342	264	.220	285.00	.712	5000.0	.686	24.9	3	B	35	2	10	10				0	2	1.0	S	M-B
R3D-329/359	433	.430	466.00	1.030	5000.0	.670	32.9	3		10	5	15	10				0	6	2.0	S	T
R3C-411/438	170	.230	250.00	.732	5000.0	.682	20.9	2	A	100	5	25	15	30	60	40				S	M
R3D-250/277	447	.270	350.00	.854	5000.0	.711	34.0	3		50	4	15	5				0	4	1.0	MS	T
R3D-318/345	468	.490	547.00	.942	5000.0	.714	20.4	3		5							0	10	1.0	MS	M
R5C-250/277	495	.380	395.00	.648	1870.0		21.7	3									1	7	3.0	S	B
R5C-328/355	401	.300	340.00	.834	5000.0	.556	24.0	3											1.0		
R5D-255/282	400	.440	490.00	.700	5000.0	.745	28.5	3									1	15	2.0		
R5D-325/352	474	.390	440.00	.850	5000.0	.635	16.4	3									1	10	2.0		
R6A-661/688	269	.280	263.00	.673	1475.0		64.4	3	B								1	20	10.0	S	T
R6C-589/616	395	.280	288.00	.886	2220.0		17.4	3									1	5	2.0	MS	M
R8C-444/471	400	.280	290.00	.921	2700.0		21.3	2	A	100	5	10	7	30	76	55				S	M
R8C-508/535	253	.200	202.00	.500	5000.0	.435	21.3	2	A	100	3	15	10	40	54	35				S	T-M
R8D-477/504	188	.320	367.00	.574	5000.0	.718	14.0	2	A	100	2	20	10	16	82	35				S	M
R8D-565/592	396	.230	254.00	.824	5000.0	.361	16.8	2	A	100	2	25	10	42	54	80				MS	B
R9A-523/550	411	.120	161.00	.921	5000.0	.577	31.1	3									1	5	2.0	S	B
R9B-449/476	293	.320	308.00	.770	5000.0	.713	47.1	3			30	2	10	5			0	5	1.0	MS	M
R9C-395/422	411	.340	363.00	2.000	5000.0	.640	33.3	3											3.0	MS	T
R9D-317/344	377	.630	394.00	.844	5000.0	.600	40.6	3											2.0	MS	M-B
R10A-320/347	466	.190	259.00	.966	5000.0	.479	14.0	3												S	B
R10B-418/455	549	.620	682.00	.761	5000.0	.794	15.1	3												MS	M
R10C-347/374	396	.250	286.00	.959	5000.0	.477	19.7	2	A	90	2	15	7	90	70	A				S	T
R10D-356/383	377	.210	268.00	1.030	5000.0	.478	18.2	3			5	15	.10			U			2.0	MS	B

APPENDIX B. MULTI-YEAR FLOE SAMPLE DATA

This appendix contains the results from the structural analysis of the tests performed on the multi-year floe ice samples. The results are grouped according to the type of test; constant-strain-rate uniaxial compression; constant-load uniaxial compression; constant-strain-rate uniaxial tension; and constant-strain-rate triaxial. Most variables have been defined in Index A with the following exceptions. In the constant-load compression data, σ is the applied stress on the sample, $\dot{\varepsilon}_{min}$ (FS) is the strain-rate minimum determined from full sample displacement, ε_f (FS) is the full sample strain at the strain-rate minimum or failure, and t_f is the time to failure.

Table B1. Multi-Year Floe

Structural
Constant Strain-Rate Uniaxial Compression Test Data

Sample Number	σ_m psi	ε_m (GL)%	t_m sec	E_i (GL)x10^6 (psi)	t_e sec	σ_e/σ_m	n o/oo	Ice type	% Columnar	Columnar grain size (mm) min	max	mean	σ:z degree	σ:c degree	Spread degree	Granular grain size (mm) min	max	mean	Failure mode type	location
$\dot{\varepsilon}=10^{-3}$ s^{-1}, T=-5°C																				
C22-129/156	1373	0.09	1.45	1.26	1.45		29.5	2A	100	2	6	4	2	88	40				L	T-M
C22-159/186	1206	0.15	1.92	0.880	1.92		35.7	2A	100	1	8	5	0	90	70				L	M
$\dot{\varepsilon}=10^{-5}$ s^{-1}, T=-5°C																				
C18-167/194	167	0.25	282	0.567	5000	0.701	36.2	2A	100	2	8	8	80		Unaligned				MS	T-M
C18-269/296	97.5	0.25	230	0.607	5000	0.734	27.0	2A	100	3	10	5	90	3	50				MS	B
$\dot{\varepsilon}=10^{-3}$ s^{-1}, T=-20°C																				
C23-213/240	1520	0.20	2.51	1.07	50.0	0.123	17.6	3	70			5	4	86	50	2	5	3	MS	M
C23-244/271	1556	0.19	1.86	0.880	50.0	0.151	15.5	2A	100			5	90		Unaligned				MS	M
$\dot{\varepsilon}=10^{-5}$ s^{-1}, T=-20°C																				
C19-165/192	543	0.19	258	1.01	5000	0.475	21.8	2A	100	1	8	4	5		Unaligned				MS	B
C18-236/263	258	0.23	90	0.718	5000	0.349	17.1	2A	100			5	60	70	30				MS	M-B
$\dot{\varepsilon}=10^{-2}$ s^{-1}, T=-20°C																				
C5-228/254	1345	0.10	0.20	0.841	0.20		11.7													
C13-236/263	1273	0.11	0.16	1.061	0.16		18.7	3					Random-Platey Structure					6		
C23-158/185	2157	0.15	0.21	1.079	0.21		22.1	3	90			6	5	85	75			3		

Table B2. Multi-Year Floe

Structural
Constant-Load Compression Test Data

Sample Number	σ_m psi	T °C	$\dot{\varepsilon}$ (FS) min sec^{-1}	ε_f(FS) %	t_f sec	n o/oo	Ice type	% Columnar	Columnar grain size (mm)			σ:z degree	σ:c degree	Spread degree	Granular grain size (mm)		
									min	max	mean				min	max	mean
Bellofram Tests																	
C22-269/296	100	-5	1.98×10^{-8}	0.311	1.04×10^{5}	16.7	3	90		Top:	8	10	80	75			
										Bottom:		82					
C18-136/163	100	-5	3.44×19^{-8}	0.311	5.40×10^{4}	36.3	3	60			7	10					3
C19-134/161	100	-20	No $\dot{\varepsilon}_{min}$			17.6	2A	100	1	10	7	5	85	70			
C14-129/156	100	-20	No $\dot{\varepsilon}_{min}$			38.7	3	80				40	81	30			
MTS Tests																	
C16-134/161	300	-5	1.00×10^{-7}	0.180	1.20×10^{4}	33.0	2A	100	3	7	5	2	88	40			
C16-073/100	600	-5	1.41×10^{-6}	0.168	9.10×10^{2}	34.7	2A	100	2	11	5	2	88	60			
C12-267/294	600	-5	2.39×10^{-4}	0.187	5.0	26.8	2A	100				90		Unaligned			
C16-165/192	600	-20	5.60×10^{-6}	0.208	2.08×10^{2}	18.9	3	85	3	6	3	0	90	70			2
C12-236/263	600	-20	6.67×10^{-5}	0.155	1.07×10^{1}	22.6	2A	100				70	90	60			

Table B3. Multi-Year Floe

Structural
Constant Strain-Rate Uniaxial Tension Test Data

Sample Number	σ_m psi	ε_m (FS)%	t_m sec	E_i (FS)x10^6 psi	t_e sec	n o/oo	Ice type	% Columnar	Columnar grain size (mm) min	max	mean	σ:z degree	σ:c degree	Spread degree	Granular grain size (mm) min	max	mean
$\dot{\varepsilon}=10^{-3}$ s^{-1}, T=-5°C																	
C17-228/255	168	0.013*	0.38	1.167*	0.38	20.9	3	65	2	5	4	85	86	50	1	5	2
C17-259/286	185	0.014*	0.41	0.657*	0.41	17.6	3	70			10	80	80	45	3	10	
C21-092/119	160	0.014	0.25	0.945	0.25	34.1	2A	100	2	12	7	7	83	70			
C22-077/104	94.6	0.009	0.17	1.751	0.17	26.6	2A	100	2	7	5	5	85	65			
$\dot{\varepsilon}=10^{-5}$ s^{-1}, T=-5°C																	
C16-224/251	169	0.025	27.6	0.849	27.6	23.7	2A	100	3	10	7	10	80	55			
C16-256/283	142	0.037	38.3	0.650	38.3	19.6	2A	100	2	10	6	24	79	60			
C16-288/315	122	0.024	22.8	0.815	22.8	24.0	3	70	2	10	5	20	71	45	2	6	4
$\dot{\varepsilon}=10^{-3}$ s^{-1}, T=-20°C																	
C15-135/162	152	0.011*	0.12	1.377*	0.12	13.0	2A	100	2	12	5	8		Unaligned			
C21-198/225	83.2	0.008	0.20	1.260	0.20	46.5	3								2	10	2
C21-154/161	154	0.012	0.24	1.283	0.24	12.5	2A	100	2	8	4	6	84	60			
$\dot{\varepsilon}=10^{-5}$ s^{-1}, T=-20°C																	
C17-126/155	189	0.018*	3.24	1.223*	3.24	12.9	2A	100	2	8	5	6	84	45			
C21-166/193	125	0.021	20.9	0.666	20.9	19.9	2A	100	2	10	6	5	85	55			
C21-266/293	164	0.023	23.2	1.047	23.2	13.9	3	90			7	80		Unaligned			
C22-236/263	124	0.028	27.5	1.247	27.5	16.7	2A	100	3	10	7	11	79	60			

*Gauge Length Data, GL = 4.0 in.

Table B4. Multi-Year Floe

Structural
Constant Strain-Rate Triaxial Compression Test Data

Sample Number	σ_m psi	ε_m (FS)%	t_m sec	E_i (FS)x10^6 psi	t_e sec	σ_e/σ_m	n o/oo	Ice type	% Columnar	Columnar grain size (mm) min	max	mean	σ:z degree	σ:c degree	Spread degree	Granular grain size (mm) min	max	mean	Failure mode type	location
$\dot{\varepsilon}=10^{-3}\ s^{-1}$, T=-5°C, σ_r/σ_a = 0.46																				
C6-228/255	1991	0.56	5.28	0.336	50	0.565	26.1	2A	100	2	10	4	12	80	40				MS	M-B
C6-259/286	1984	0.61	5.97	0.553	50	0.491	22.6	2A	100	2	11	8	14	78	55					
C7-129/154	>3716	0.81		0.737	50		20.0	2A	100	2	6	4	4		Unaligned					
C7-267/294	>2041			0.869	50		23.3	2A	100	1	10	5	2	88	80				MS	T
C24-138/165	2865	0.73	7.25	0.907	50	0.361	52.2	2A	100	1	11	4	2	88	80				MS	M
C24-268/295	1474	0.89	8.80	0.394	50	0.680	31.6	3	75	2	10	7	56	32	35				MS	M
$\dot{\varepsilon}=10^{-3}\ s^{-1}$, T=-5°C, σ_r/σ_a = 0.68																				
C6-132/158	>3716	1.08		0.700			28.7	2A	100	1	11	5	4	86	90					
C19-271/298	3099	1.59	16.2	0.700	50	0.810	22.0	3				10	70		Unaligned	2	6	4	MS	M
C20-188/215	2772	1.61	16.1	0.569	50	0.641	34.6	3	90				71	20	35				MS	M-B
C20-238/265	>3716			0.639			29.6	2A	100	2	18	6	5		Unaligned					
$\dot{\varepsilon}=10^{-5}\ s^{-1}$, T=-5°C, σ_r/σ_a = 0.46																				
C7-155/180	1148	0.42	416	0.760	5000	0.423	23.8	2A	100	2	10	4	5	85	90				MS	T-B
C7-236/263	479	0.47	467	0.715	5000	0.674	25.8	2A	100	3	11	8	15	80	60				MS	T-B
C24-072/099	1512	0.53	536	0.509	5000	0.347	22.4	2A	100	2	12	4	4	86	90				MS	T
C24-237/264	927	0.69	562	0.268	5000	0.721	32.5	3					4	86	100	1	5	2	MS	M

Table B4 (Con't).

Sample Number	σ_m psi	ε_m (FS)%	t_m sec	E_i (FS)x10^6 psi	t_e sec	σ_e/σ_m	n o/oo	Ice type	% Columnar	Columnar grain size (mm)			σ:z degree	σ:c degree	Spread degree	Granular grain size (mm)			Failure mode	
										min	max	mean				min	max	mean	type	location
$\dot{\varepsilon}=10^{-5}$ s^{-1}, T=-5°C, σ_r/σ_a = 0.68																				
C13-267/294	758	0.88	880	0.328	5000	0.697	40.7	2A	100			7	79	90	65				MS	T-M
C14-267/294	602	1.03	927	0.356	5000	0.902	38.9	2A	100				90	65	80				MS	T-B
C19-081/108	2535	0.67	670	0.636	5000	0.408	24.1	2A	100	2	12	5	2	88	60				MS	T-B
C24-164/196	1197	0.82	845	0.439	5000	0.733	39.3	2A	100	2	10	5	4	86	80				MS	M
$\dot{\varepsilon}=10^{-3}$ s^{-1}, T=-20°C, σ_r/σ_a = 0.46																				
C12-072/099	>3716			0.590			13.2	2A	100	2	12	6	5	85	100					
C14-236/263	3329	1.02	10.54	0.543	50	0.458	18.8	2A	100				60		Unaligned				MS	T
$\dot{\varepsilon}=10^{-5}$ s^{-1}, T=-20°C, σ_r/σ_a = 0.46																				
C18-072/099	2212	0.60	596	0.369	5000	0.312	7.3	3	80	2	10	7	5	85	65			3	MS	T
C19-240/267	1429	0.76	762	0.188	5000	0.564	25.0	3				5	6	86				2	MS	T-M
$\dot{\varepsilon}=10^{-5}$ s^{-1}, T=-20°C, σ_r/σ_a = 0.68																				
C6-163/189	2527	3.21	3190	0.444	5000	0.862	15.8	2A	100				6	84	80				MS	T-B
C20-269/296	2320	1.72	1705	0.340	5000	0.804	16.5	3	80	2	12	7	7		Unaligned	1	5	3	MS	T